(This is a sample cover image for this issue. The actual cover is not yet available at this time.)

International Journal of Greenhouse Gas Control 12 (2013) 399–418

Contents lists available at SciVerse ScienceDirect

International Journal of Greenhouse Gas Control

journal homepage: www.elsevier.com/locate/ijggc

The geology and water chemistry of the Hellisheidi, SW-Iceland carbon storage site

Helgi A. Alfredsson[a,b,*], Eric H. Oelkers[a,b], Björn S. Hardarsson[c], Hjalti Franzson[c], Einar Gunnlaugsson[d], Sigurdur R. Gislason[a]

[a] Institute of Earth Sciences, University of Iceland, Sturlugötu 7, 101 Reykjavík, Iceland
[b] GET, CNRS/UMR 5563-Université Paul Sabatier, 14 rue Edouard Belin, 31400 Toulouse, France
[c] Iceland GeoSurvey, Grensásvegi 9, 108 Reykjavík, Iceland
[d] Reykjavík Energy, Baejarhálsi 1, 110 Reykjavík, Iceland

ARTICLE INFO

Article history:
Received 23 November 2011
Received in revised form 18 October 2012
Accepted 19 November 2012

Keywords:
CO_2 sequestration
Mineral carbonation
CO_2 Carbonatization
Geochemical monitoring
Basalts
CarbFix

ABSTRACT

The subsurface rocks at the Hellisheidi carbon injection site are primarily olivine tholeiite basalts consisting of lava flows and hyaloclastite formations. The hyaloclastites are low permeability glassy rocks formed under ice and melt water during glaciations that serve as the cap rock at the injection site; the boundaries between hyaloclastites and lava flows and those between individual lava flows boundaries are preferential fluid flow pathways. Some alteration is observed in the hyaloclastite cap rock situated at 100–300 m depth consisting primarily of smectite, calcite, Ca-rich zeolites, and poorly crystalline iron-hydroxides. Alteration increases with depth. These alteration phases lower the porosity and permeability of these rocks. Carbon dioxide injection will be targeted at a lava flow sequence at 400–800 m depth with the main aquifer located at 530 m depth. Loss on ignition suggests that over 80% of the primary rocks in the target zone are currently unaltered. The target zone rocks are rich in the divalent cations capable of forming carbonates; on average 6 moles of divalent cations are present per 1 kg of rock.

The water in the target zone ranges in temperature from 15 to 35 °C; the *in situ* pH ranges from 8.4 to 9.8. The partial pressure of CO_2 and O_2 suggest that the water in this system is isolated from the atmosphere. The concentration of Ca and Mg in these waters are limited by secondary mineral precipitation. All the waters are supersaturated with Ca-zeolite, analcime, Ca–Mg–Fe smectite, calcite, and aragonite, and some are supersaturated with respect to dolomite and Fe–Mg carbonates.

Pure commercial CO_2 and a 75%–24.2%–0.8% mixture of CO_2–H_2S–H_2 gases will be dissolved into water prior to its injection into this system. The injected water will have a temperature of ~25 °C and be equilibrated with ~25 bar pressure of the CO_2 gas, and ~14 bar pressure of the CO_2–H_2S–H_2 mixture. The injected gas will have total CO_2 concentrations of ~0.8–0.42 mole/kg H_2O and a pH of 3.7–4.0, depending on the H_2S concentration of the injected gas. All host rock minerals and glass will be strongly undersaturated with respect to the gas charged injection waters. The water will therefore create porosity in the near vicinity of the injection by dissolving primary and secondary minerals. Further from the injection, secondary minerals will precipitate, potentially clogging the system. Reaction path modeling shows that 1–2 moles of basaltic glass are needed to lower the injected CO_2 concentration down to natural pre-injection concentrations, but less than 1 mole is needed for the sequestered H_2S. Major carbonates formed were Ca–Mg–Fe–carbonate and dolomite at pH <5, whereas ankerite and calcite formed later at higher pH. Associated minerals at lower pH were chalcedony, kaolinite and iron hydroxide, followed by smectite and zeolites at higher pH. Modeling result suggest that the first sulfur bearing phase to precipitate is elemental sulfur, followed by greigite and mackinowite upon further basalt dissolution.

1. Introduction

1.1. Carbon storage in mafic rocks

The reduction of CO_2 emissions to the atmosphere is one of the main challenges of this century. One solution to this challenge is carbon capture and storage (Lackner et al., 1995; Broecker and Kunzig, 2008; Oelkers and Cole, 2008). This technique may include

* Corresponding author at: Institute of Earth Sciences, University of Iceland, Sturlugötu 7, 101 Reykjavík, Iceland. Tel.: +354 5255248; fax: +354 5254499.
E-mail address: haa4@hi.is (H.A. Alfredsson).

1750-5836/$ – see front matter © 2012 Elsevier Ltd. All rights reserved.
http://dx.doi.org/10.1016/j.ijggc.2012.11.019

the injection of CO_2 into deep geologic formations because the estimated storage capacity is large, and many promising geological formations are located close to large emission sources. (IPCC, 2005; Le Quéré et al., 2009). If injected at depths greater than 800 m, CO_2 is supercritical, yet it is still buoyant. The long-term geological storage of buoyant supercritical CO_2 requires high integrity cap-rock, which can be degraded through either fluid/rock interaction and/or fracturing resulting from pressure changes during and after injection (*e.g.* Rutqvist et al., 2007). Some of the risk associated with CO_2 buoyancy can be overcome by its dissolution into water during its injection (Gislason et al., 2010). Once dissolved, CO_2 is no longer buoyant, improving security and helping to promote carbonation of reactive host rocks. The CO_2 mineralization of reactive silicate rocks, involves the dissolution of the rock, which consumes protons from the aqueous phase, and the release of divalent metal cations, primarily Ca^{2+}, Mg^{2+}, Fe^{2+} and Mn^{2+}, to the fluid. These ions can react with dissolved CO_2 to precipitate carbonate minerals. The rate-limiting step for this mineralization is thought to be the release of divalent cations (*cf*, Oelkers et al., 2008). Because of their reactivity and abundance, basalt and ultramafic rocks are the most promising silicates for mineral carbonation (McGrail et al., 2006; Wolff-Boenisch et al., 2006; Goldberg et al., 2008; Oelkers et al., 2008; Kelemen and Matter, 2008; Matter and Kelemen, 2009; Gislason et al., 2010; Oelkers and Gislason, 2010). This potential has lead to a large number of field and experimental studies to assess the feasibility of *in situ* mineral sequestration in mafic rocks (Flaathen and Gislason, 2007; Flaathen et al., 2008, 2009, 2010, 2011; Alfredsson et al., 2008, 2011; Gudbrandsson et al., 2008, 2011; Goldberg et al., 2008, 2010; Gysi and Stefánsson, 2008, 2011, 2012; Khalilabad et al., 2008; Stockmann et al., 2008, 2011; Aradóttir et al., 2009, 2011, 2012; Schaef and McGrail, 2009; Schaef et al., 2010; Matter et al., 2011; Wolff-Boenish et al., 2011). Building upon these past studies, this manuscript presents a case study of a basaltic rock hosted geological carbon storage site and assessment of the potential reactions that might occur in response to pure CO_2 and CO_2–H_2S–H_2 injection.

2. Description of study site

This study is focussed on the basaltic rocks located adjacent to the Hellisheidi geothermal power plant located in SW Iceland, at 260–290 m.a.s.l., 30 km east of Reykjavík (see Fig. 1). The power plant currently produces 40,000 tons of CO_2 and 16,000 tons of H_2S per year. These gases are a by-product of geothermal energy production and are of magmatic origin. Subsequently, a CO_2–H_2S–H_2 gas mixture, following its separation from other geothermal gases, will be transported in a pipeline to the injection site shown in Fig. 2. A short-term injection test was performed at this site in early 2012, where 175 tons of pure commercial CO_2 was injected. This short-term test will be followed by a 1200 ton injection of a geothermal CO_2–H_2S–H_2 gas mixture over a 6-month period. In both cases the gases will be pumped with water down to 500 m. The gases will be fully dissolved within the injection well, resulting in a single fluid phase entering the storage formation. This gas charged water is acidic and thus reactive. The Hellisheidi site has been outfitted with one 2000 m deep injection well, ten monitoring wells ranging from 50 to 1300 m in depth, and various injection and monitoring equipment (Gislason et al., 2010; Matter et al., 2011; Alfredsson et al., 2011; Aradóttir et al., 2011).

The Hellisheidi site is located on a triple junction between the volcanic zones of Reykjanes Peninsula (RP), Western Volcanic Zone (WVZ), and South Iceland Seismic Zone (SISZ) as shown in Fig. 1a (Hardarson et al., 2010). The Hellisheidi site is dominated by basaltic and ultrabasic lava flows and glassy hyaloclastites, fissure swarms, grabens, and geothermal systems (*i.e.* Einarsson, 1960; Saemundsson, 1967, 2003; Jakobsson et al., 1977; Hardarson et al., 2010). The injection site sits on the western flank of the Hengill central volcano and fissure swarm (Fig. 1b). The Hengill system contains rocks ranging in age from >400,000 to 0 AD (Saemundsson, 1995; Franzson et al., 2005). The volcanic rocks formed during the interglacials are mostly lava flows piled up in the surrounding lowlands, with rugged glassy (scoria) tops and bottoms but more crystalline interiors. The primary minerals are predominantly plagioclase (An90-30), olivine (Fo90-80), where early olivines contain occasional chromium spinel inclusions, clinopyroxene (commonly augite), magnetite-ilmenite, and interstitial glass (Jakobsson et al., 1977; Oskarsson et al., 1982; Larsson et al., 2002). The initial porosity of the lava flows range from 5 to 40% (Franzson et al., 2008), mostly present in the glassy tops and bottoms of these flows. Some porosity is also contained in cooling cracks and columnar jointing. Alteration of the basaltic lava flows commonly leads to smectite and zeolite precipitation and a decrease in porosity to 1–10% (Sigurdsson and Stefánsson, 1994). Younger cracks and faults, due to seismicity can increase the porosity.

The volcanic rocks formed during the glacial epochs are heterogeneous, glassy, and/or poorly crystalline (pillow-lava) material often referred to as hyaloclastites ("broken glass") (Jones, 1966; Moore and Calk, 1991; Jakobsson and Gudmundsson, 2008). The hyaloclastite formations are formed when sub-glacial eruptions melt the ice. The lava piles up as pillow lava; higher up in the pile, broken pillow breccia forms a structure surrounded by ice. When the pile has grown to shallower depth in the meltwater, a phreato-magmatic activity occurs and the magma fragments, forming a layer of glassy rock with high initial porosity on top of the pillow lava. Fragmentation stops if the vent works its way out of the melt water (Gislason et al., 2011), and lava is formed at the top of the hyaloclastite formation (Moore and Calk, 1991).

Initially the glassy hyaloclastite material has porosity of up to 60% (*e.g.* Franzson et al., 2010) and is reactive (Gislason et al., 2002; Gislason and Oelkers, 2003). Compaction, dissolution, and secondary minerals rapidly fill the macro-pores (Jakobsson and Moore, 1986; Gislason et al., 2002; Frolova et al., 2005), but at the same time, >30 μm micro-pores form within the secondary phases (Franzson et al., 2010). This process lowers the permeability dramatically. This first glass alteration is often referred to as palagonitization (Jakobsson and Moore, 1986 and references therein). Palagonite is distinguished by the presence of amorphous and/or crypto-crystalline alteration-rims on the surfaces of the glass-grains (Stroncik and Schmincke, 2001). The final secondary products of palagonitization are smectites and zeolites (Crovisier et al., 1992; Stroncik and Schmincke, 2001).

High temperature geothermal systems are located both north and south of the Hengill central volcano (see Fig. 1, Saemundsson, 1995). The highest measured geothermal gradient is 170 °C/km (Björnsson, 2005). The geothermal gradient decreases with distance away from the high-temperature geothermal systems. At the injection site this gradient is 80 °C/km. Groundwater flow in the top tens of meters is to southwest, but 1 km north of the injection site groundwater flows toward the west (Gíslason, 2003; Aradóttir et al., 2011). Water flow in the lower part of the system, is focussed in lava flows located at 400–800 m depth. This flow is slow, on the order of 25 m per year (Aradóttir et al., 2011, 2012) and the hydraulic head decreases toward southwest. Hydrological models, pump tests and tracer tests, suggest that the effective matrix porosity of this lava formation is 8.5% (Aradóttir et al., 2012). The Cl, B, ^{18}O, and deuterium concentrations of the geothermal waters, groundwaters, and precipitation in Iceland have been used to trace the origin of the groundwaters, their flow paths, and water/rock interaction (Árnason, 1976; Gislason and Eugster, 1987b; Sigurdsson and Einarsson, 1988;

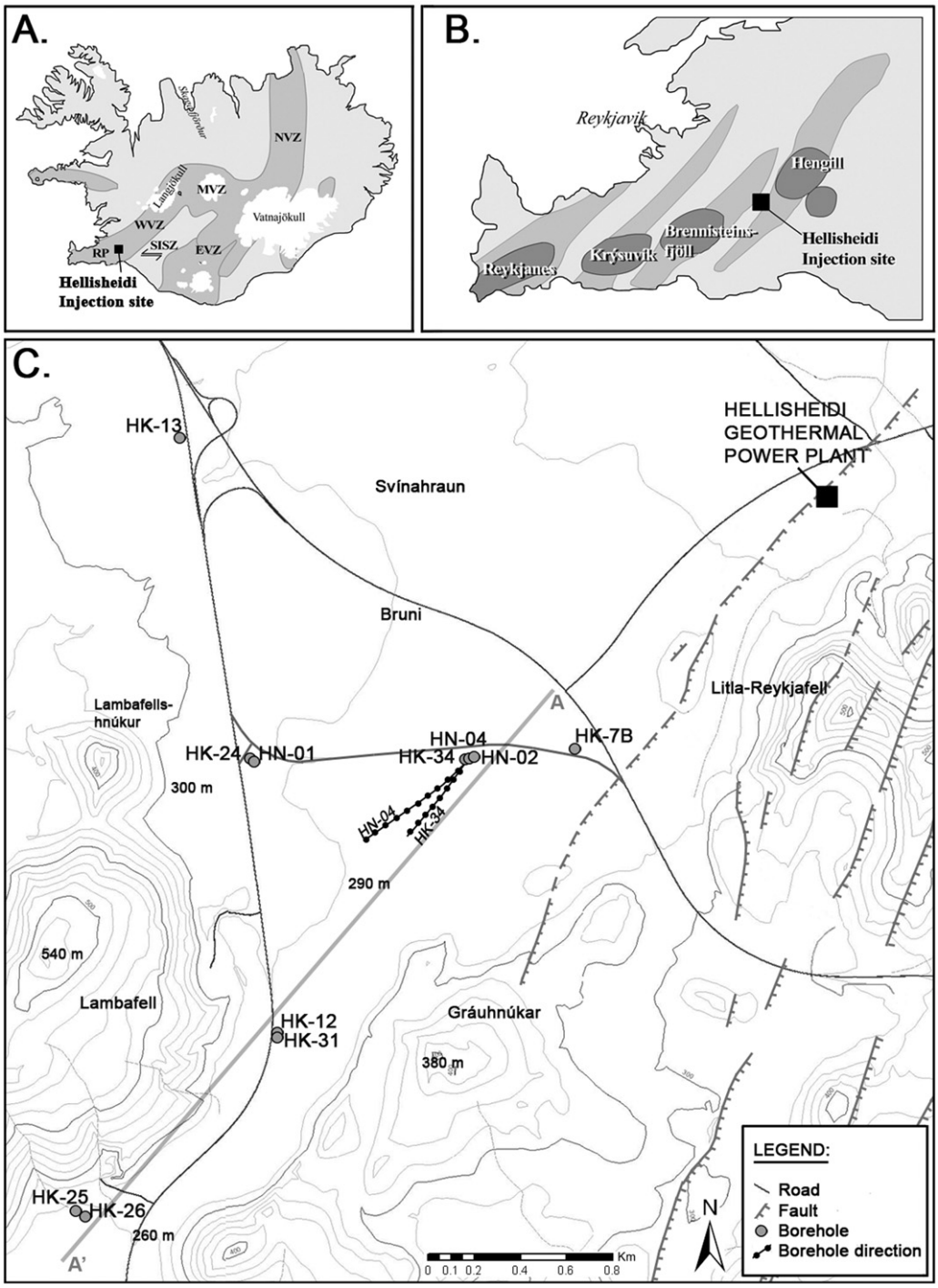

Fig. 1. Maps showing location of the study area (a) Map showing active volcanic zones in Iceland: RP = Reykjanes Peninsula, WVZ = Western Volcanic Zone, SISZ = South Iceland Seismic Zone, MVZ = Mid-Iceland Volcanic Zone, EVZ = Eastern Volcanic Zone and NVZ = Northern Volcanic Zone. (b) Map showing location of central volcanoes (dark gray) on Reykjanes Peninsula and associated fissure swarms (gray). (c) Map of the CO_2 injection site in, Hellisheidi, SW-Iceland. The CarbFix wells are shown as labeled gray dots. Mapped bedrock faults are located toward east and are part of the Hengill fissure swarm. The cross section shown in Figs. 2 and 4 is marked A-A′.

Sveinbjörnsdóttir and Johnsen, 1992; Arnórsson and Andrésdóttir, 1995). The Cl concentration of the rainwater at Hellisheidi is about 0.2–0.3 mmol/L but further inland at the Langjökull glacier it is about 0.03–0.06 mmol/L (Sigurdsson and Einarsson, 1988; Gislason et al., 2000). The deuterium and ^{18}O concentration of the local rainwater at the Hellisheidi site is on average −56‰ and −8‰ respectively, but it is −70‰ and −10‰ in the Langjökull glacier region (Sveinbjörnsdóttir and Johnsen, 1992).

3. Methods

3.1. Stratigraphy

The samples used for determining stratigraphy consisted of cuttings collected at 2 m depth intervals during drilling of the wells; the location of the wells is shown in Fig. 1. The uncertainty in the sampling depth was variable; the uncertainty in depths

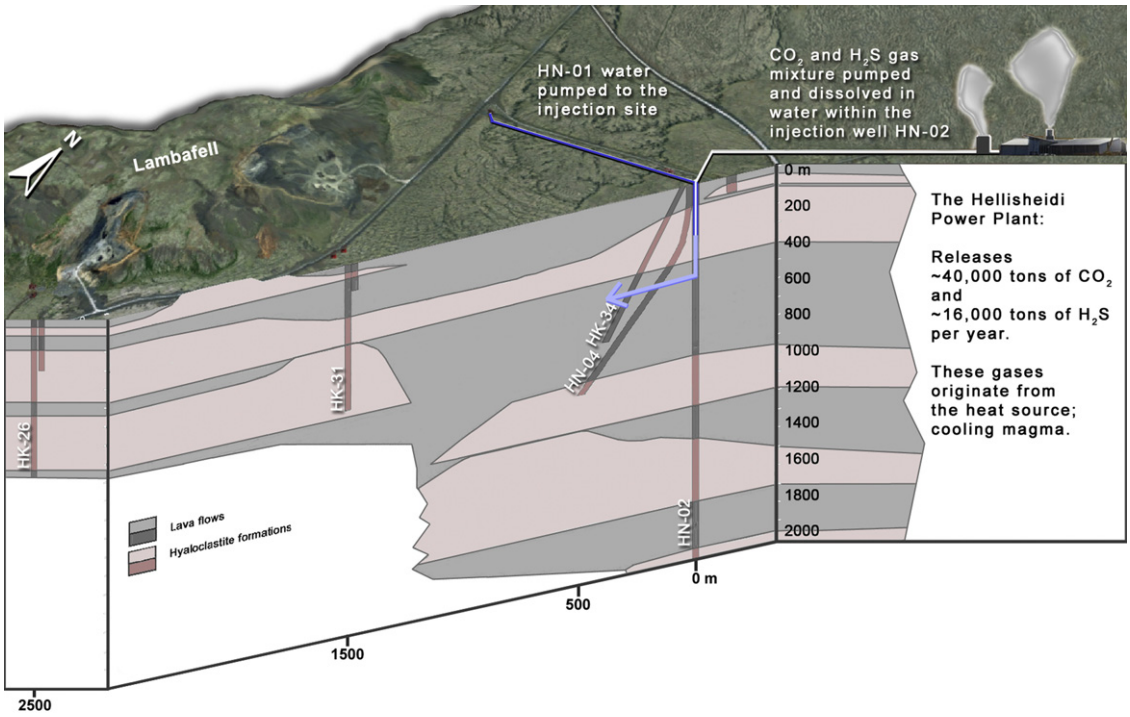

Fig. 2. Geological cross section of the injection site. The CO_2 will be separated from other geothermal gases at the power plant, and pumped toward the injection site and mixed with water from well HN-1 within the injection well HN-2. The gas charged waters enters the basaltic formations as single phase; water phase.

estimated for samples collected from depths of less than 500 m was 1 m, at greater depths this uncertainty was ~2–5 m (Hardarson et al., 2007). Individual drill cuttings were studied with a binocular microscope and X-ray diffraction (XRD) to define rock type and mineralogy. Basaltic lava flows tend to form flat horizontal formations, whereas hyaloclastites tend to form elongated high-standing ridges, such as the Lambafell and Gráuhnúkar formations shown in Figs. 1 and 2. The Hengill volcanic system, including the Hellisheidi site, is a narrow and very active volcanic system consisting of a continuous stratigraphic series covering the inter-glacial and glacial periods for the last 400 ka (*e.g.* Franzson et al., 2005). Because of the continuous record, the age of each inter-glacial and glacial formation can be estimated by simply counting the periods.

3.2. The XRD and microscopic analysis

Samples of the secondary mineral phases were collected from the drill cuttings from wells HN-2 and HK-31. The samples were powdered with an agate mortar and pestle, then analyzed by XRD using a Bruker AXS D8 Focus diffractometer equipped with a Bragg-Brentano goniometer and a Cu anode lamp with a NaI crystal type scintillation counter. These results were used to validate microscopic analysis of samples collected from the well HK-31 as reported by Alfredsson (2007).

3.3. Whole-rock chemical analysis

Whole-rock chemical analyses were performed using X-ray fluorescence (XRF). The samples were both glassy and crystalline, and collected from various depths in the wells of the study area. Fifty drill-cutting samples were prepared for chemical analysis. All the samples were cleaned of external material such as drilling mica and mud. In some samples, primary basaltic rock-grains were handpicked to represent "fresh" rock, to check for any influence of secondary phases on rock composition. Rock samples were powdered in an agate shatter box and analyzed for major and trace elements using a Panalytical PW2404 wavelength-dispersive sequential X-ray spectrometer at the University of Edinburgh. The loss on ignition (LOI) was recorded during the ignition process to assess sample alteration.

To calculate elemental ratios, the chlorine and fluorine contents of the Hellisheidi basalts were determined using the K_2O–Cl correlation for Reykjanes peninsula rocks, described by Sigvaldason and Óskarsson (1976) and the K_2O–F correlation for the same area obtained from Sigvaldason and Óskarsson (1986). The Cl concentrations were on average 195 ppm and the F content 290 ppm. Similarly, B was estimated to be around 1–2 ppm (Arnórsson and Andrésdóttir, 1995), C content was estimated to be around 500 ppm (Sveinbjörnsdóttir et al., 1995) and S concentration was estimated to be approximately 800 ppm (Moore and Fabbi, 1971).

3.4. Water sampling and analysis

Water samples from all wells in the study area were collected for chemical analysis every two months from July 2008 to November 2010. The water samples were filtered on site through 0.2 μm Millipore cellulose acetate filters using silicon tubing, and a 140 mm Sartorius filter holder, connected directly to the well head. Polypropylene bottles were used to collect samples for cation- and trace metal samples, but low-density polyethylene bottles were used to collect samples for other dissolved metals. Amber glass bottles were used to collect samples for pH and alkalinity measurements. Sampling took place after at least 24 hours of continuous pumping at around 1 L/s with a down-hole pump from the 800 to 1300 m deep wells other than HN-1, and after 2–5 h of continuous pumping at 0.3 L/s with a portable down-hole pump from the 50–200 m deep wells. The HN-1 well was fitted with a down-hole pump producing water at around 70 L/s (Khalilabad et al., 2008). This well was pumped only for one hour prior to sampling. This pre-sample pumping ensured that the samples represented fresh groundwater rather than stagnant well water.

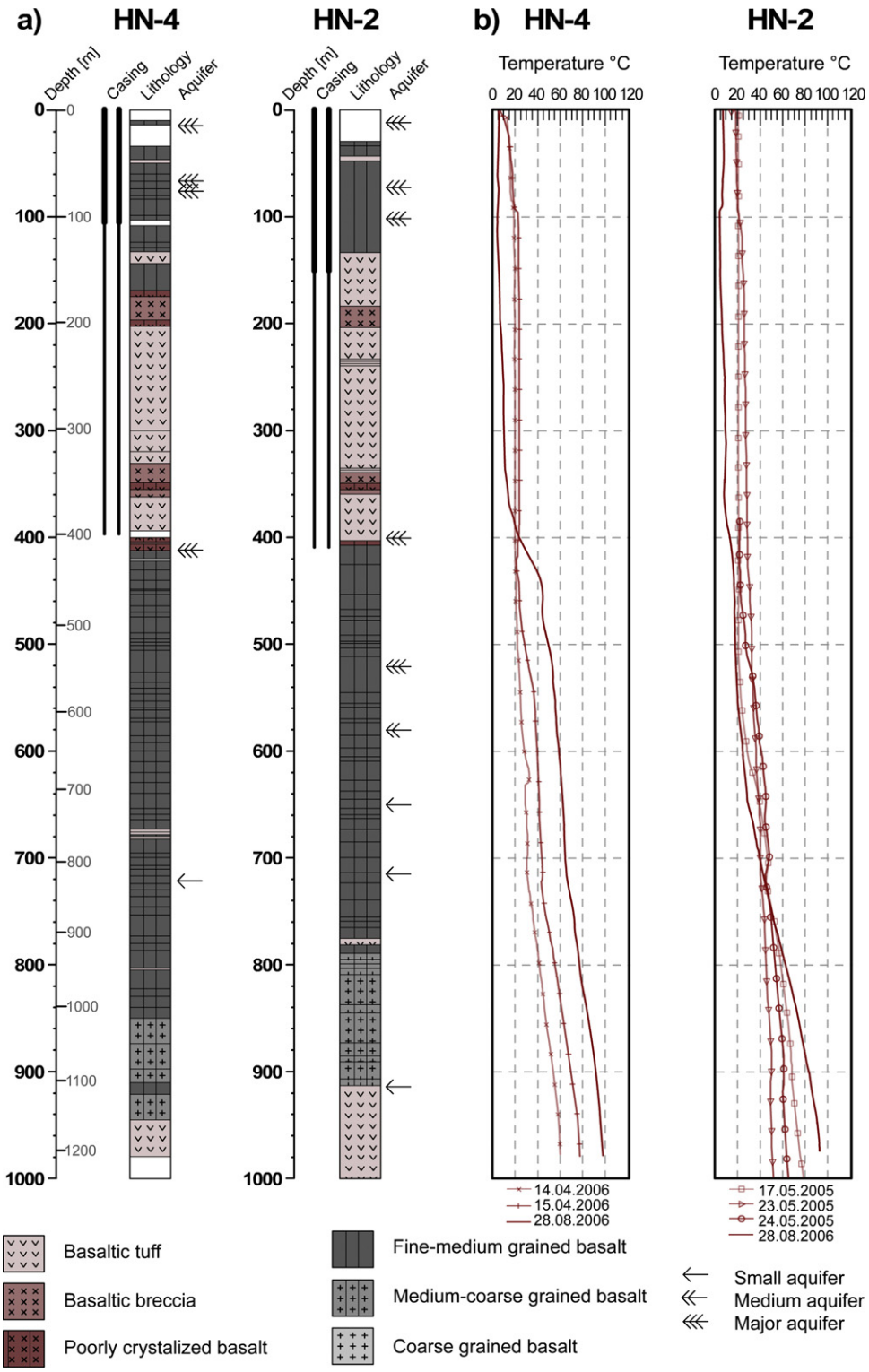

Fig. 3. (a) Lithology, casing, and possible aquifer locations as a function of depth in the HN-4 monitoring well and the HN-2 injection well. The glassy hyaloclastite formation is shown with brown color but the lava formation with gray color. Fine to coarse grained basalts refer to the crystal size of the basaltic lavas. Basaltic tuff, breccia and poorly crystallized basalts are common in the hyaloclastite formations (see Section 4.1). (b) Temperature logs of the same wells. All graphs are plotted with true vertical depth down to 1000 m, but for HN-4 the well-length is shown in gray font on the right site of the depth scale.

Modified from Helgadottir et al. (2009), Thorarinsson et al. (2006), and Axelsson and Gunnarsson (2009). (For interpretation of the references to color in this figure legend, the reader is referred to the web version of this article.)

Water samples collected for major and trace element analysis were acidified by using Suprapur® HNO_3, 1% (v/v). Temperature and conductivity were measured at the sampling site. Dissolved oxygen was fixed at the wellhead and later determined by Winkler titration. Dissolved hydrogen sulphide was measured by titration in the field using mercury and dithizone as an indicator (Arnórsson et al., 2000, 2006). The pH was determined in the laboratory a few hours after sampling with an Eutech Instruments™ CyberScan pH 110 electrode. Total dissolved inorganic carbon (DIC) was analyzed by two methods. First by pH and alkalinity titrations using the

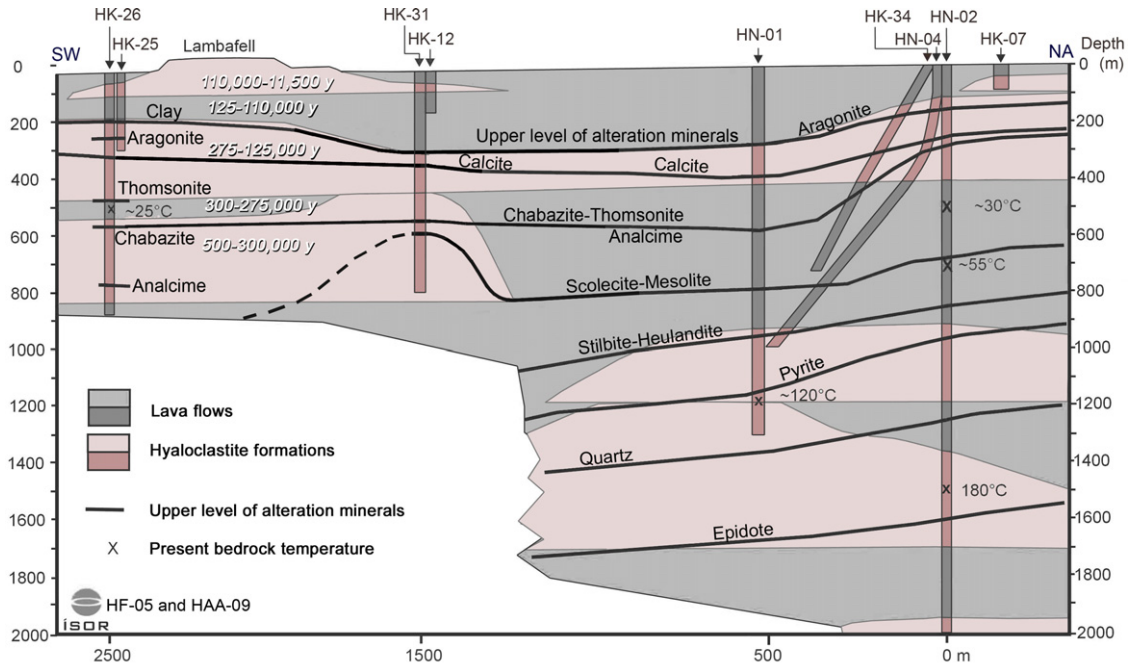

Fig. 4. Geologic cross section showing the stratigraphy of the Hellisheidi, SW-Iceland injection site (see location on Fig. 1). The location of the CarbFix wells are shown in the figure; HN-2 is the injection well, HN-1 is the water source well (1 km toward west) and HN-4, HK-34, HK-31, HK-25, HK-7b, HK-12 and HK-25 are monitoring wells. The major stratigraphy consists of hyaloclastite basalt formations (brown) and crystalline basalt formations (gray). Estimated ages of the rocks are provided in the figure. The first appearances of secondary mineral formations are shown as black lines. The bedrock temperature at around 500 m depth is *ca.* 30 °C in HN-2 rising to 180 °C at around 1500 m depth.

Gran function to determine the end point of the titration (Stumm and Morgan, 1996), and secondly by ion chromatograpy using a DIONEX, ICS-2000 (Stefánsson et al., 2007). Dissolved F^-, Cl^-, and SO_4^{-2} concentrations were quantified using a DIONEX, ICS-2000 ion chromatograph. Cations and trace metals were analyzed by ICP-OES. Rare earth elements (REE) and some other trace metals were measured by ICP-SFMS at ALS Scandinavia, Luleå, Sweden. Analytical measurements had an inter-laboratory reproducibility of within 5.2%. The average charge balance of the samples was within 2.4% as calculated using the PHREEQC speciation program (Parkhurst and Appelo, 1999).

3.5. Modeling

Modeling of the water chemistry, including calculation of percent error in charge balance, the effect of temperature on chemical speciation, the saturation state of the water with respect to mineral and gas phases, and predictions of the aqueous chemistry during CO_2 injection was performed using PHREEQC (Parkhurst and Appelo, 1999). The standard PHREEQC database with additional data from Gysi and Stefánsson (2011) was used for these model calculations.

4. Results

4.1. Bedrock stratigraphy and alteration

The lithology of the HN-2 injection well and the monitoring well closest to this well, HN-4, is shown in Fig. 3a. The boreholes are cased down to 410 and 400 m depth, respectively. The distance between HN-2 and HN-4 increases with depth as HN-4 is diverted toward southwest as shown in Figs. 1c and 2. HN-4 is 10 m west of HN-2 at the surface, 60 m SW of the HN-2 at 400 m depth, and 125 m at 520 m depth.

A sequence of aquifer-bearing fine-grained (crystals ≤1 mm) basaltic lava flows was observed from the surface down to 130 m depth in both wells. A hyaloclastite formation containing glassy basaltic tuff layers, consisting of consolidated volcanic ash, is located at depths from 130 to 400 m. This formation also contains (1) layers of breccia consisting of consolidated volcanic ash and poorly crystallized basalt-fragments, and (2) poorly crystallized basalts including pillow lavas. A loss of drill-fluid was observed at the base of this hyaloclastite during the drilling in both wells, indicating the presence of a major aquifer. Below 400 m, a thick pile of fine to medium grained basaltic lava flows containing 1–5 mm diameter crystals was observed down to around 800 m depth. A possible major aquifer indicated by the loss of drill-fluid is present at 520 m depth in HN-2. Several other small to medium aquifers were observed at greater depths. At depths from 800 to around 915 m in HN-2 and 945 m in HN-4, a medium to coarse grained basalt containing 5 mm–3 cm diameter crystals is present. A second hyaloclastite formation is located at greater depths. Carbon dioxide injection is aimed at the aquifer located at 520 m depth in HN-2.

The temperature logs are shown in Fig. 3b. The measured temperature at 530 m depth ranged from 18 to 30 °C during 2005–2006 in the HN-2 injection well and 20–30 °C in 2006 at 410 m depth in HN-4. Note that these are the depths of the main feed-zones in the wells (Khalilabad et al., 2008; Aradóttir et al., 2012).

The overall stratigraphy of the rocks at the study area is shown as a NE–SW cross-section in Fig. 4. The surface is at 290 m.a.s.l. in the NE end of the section but 260 m.a.s.l. at the SW end. The sequence of the alteration minerals, shown in Figs. 4 and 5, and Table 1, indicate a progressive increase in alteration temperature with depth, spanning the smectite-zeolite alteration zone down to 800–1000 m depth (Kristmannsdóttir and Tómasson, 1978; Franzson et al., 2008). Microscopic and XRD analysis show that the major alteration phases at the depth of the CO_2 injection (~500 m) are pore filling Ca–Mg–Fe–smectite, Ca-rich zeolites (mesolite and chabazite) and

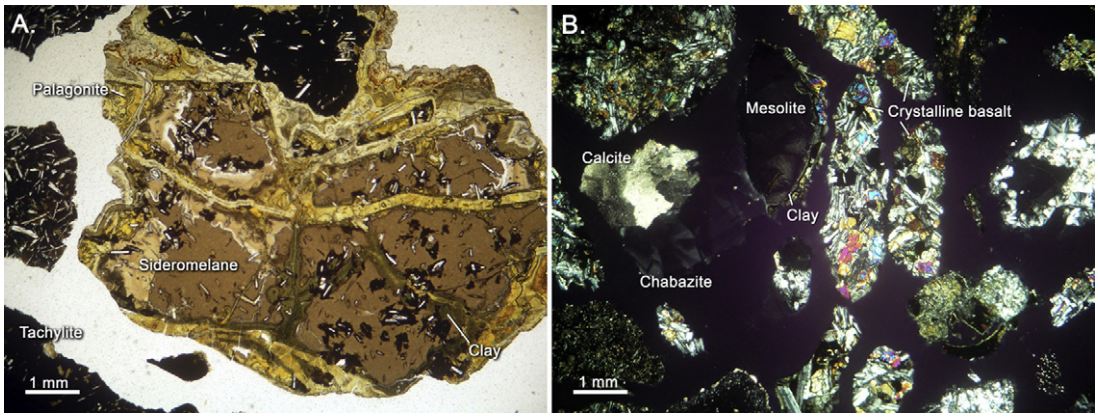

Fig. 5. Images of the drill-cuttings from the HK-31 monitoring well obtained using a petrographic microscope. (a) Slightly altered basaltic glass grains, consisting of tachylite in black and sideromelane (unaltered glass) in brown, taken from 452 m depth and viewed in plain polarized light. Altered glass appears as yellow palagonite on the grain surface and in cracks with secondary clay present. (b) Crystalline basalt grains obtained from 718 m depth in the same borehole, viewed in crossed polarized light. Observed secondary minerals were pore filling clays, zeolites, and calcite.

Table 1
Secondary minerals observed in the study area.

Secondary mineral	Chemical formula/detected formula (by XRD)	Depth of appearance (m)	Microscopic confirmation	XRD confirmation
Smectite (*e.g.* saponite)	$Ca_{0.1}Na_{0.1}Mg_{2.25}Fe^{2+}{}_{0.75}Si_3AlO_{10}(OH)_2{\cdot}4(H_2O)$	120–300	X	X
Aragonite	$CaCO_3$	150–250		
Calcite	$CaCO_3/CaCO_3$	220–400	X	X
Analcime	$NaAlSi_2O_6{\cdot}H_2O/Na_{15.76}Al_{15.26}Si_{32.74}O_{96}{\cdot}16H_2O$	250–760		X
Chabazite–Ca	$NaCa_2Al_5Si_{13}O_{36}{\cdot}14H_2O/Ca_2Al_4Si_8O_{24}{\cdot}12H_2O$	250–590	X	X
Thomsonite	$NaCa_2Al_5Si_5O_{10}{\cdot}6H_2O/NaCa_2Al_5Si_5O_{20}{\cdot}6H_2O$	250–590	X	X
Garronite	$Na_2Ca_5Al_{12}Si_{20}O_{64}{\cdot}27(H_2O)/NaCa_{2.5}(Si_{10}Al_6)O_{32}{\cdot}14H_2O$	300–500		X
Scolesite	$CaAl_2Si_3O_{10}{\cdot}3H_2O$	600–800	X	
Mesolite	$Na_2Ca_2Al_6Si_9O_{30}{\cdot}8H_2O/Na_2Ca_2Al_6Si_9O_{30}{\cdot}8H_2O$	600–800	X	X
Stilbite–Ca	$NaCa_4(Al_9Si_{27}O_{72}){\cdot}28H_2O/Na_{1.76}Ca_{4.00}(Al_{10.29}Si_{25.71}O_{72}){\cdot}29{\cdot}4H_2O$	820–950	X	X
Heulandite–Ca	$(Ca,Na)_{2-3}Al_3(Al,Si)_2Si_{13}O_{36}{\cdot}12H_2O/Ca_{1.94}(Na_{0.91}Ca_{1.76})(Na_{0.39}K_{0.13})(Al_{8.9}Si_{27.1}O_{72}){\cdot}24{\cdot}76H_2O$	820–950	X	X

calcite. In general, the alteration minerals were observed at shallower depths in the eastern part of the study site, probably due to more frequent bedrock faulting and elevated geothermal gradients. Formation temperatures, estimated from the sequence of the alteration minerals, ranged from 25 °C at a depth of 500 m to 180 °C at a depth of 1500 m. These temperatures are similar to those measured in the well-water of HN-2 and HN-4.

The estimated ages of the first 800 m of rock are shown in the upper left of the section in Fig. 4. The youngest rocks are the lava flows enclosing the Lambafell hyaloclastite ridge; these rocks are estimated to be 2000–5000 years old. The Lambafell hyaloclastite ridge was formed during the last glaciation but the hyaloclastite formation at 600–800 m depth could have formed 300,000–500,000 years ago.

4.2. Rock chemistry

Fifty rock samples were analyzed for major and trace elements; the results of these analyses are given in Table 2. A total of 30 chemical constituents were measured. The silica compositions, as plotted in Fig. 6 range from about 45 to 49% SiO_2. The overall chemical composition range spans from picrite to tholeiite (*e.g.* Jakobsson, 1980). The majority of the rocks are of olivine tholeiite composition. The variation with depth of selected element concentrations and loss on ignition (LOI) is shown in Fig. 7. The sum of the concentrations of the major divalent cation oxides CaO, MgO, and FeO, ranged from 25 to 33% of the rocks and MnO ranged from 0.16–0.28%. The concentration of CrO, a potential pollutant ranged from 0.001 to 0.01%.

The LOI is a direct measure of the alteration state of the rocks. Studies of alteration states and measured LOI of basalts from several central volcanoes in Iceland showed a clear correlation between the unaltered primary rock content and measured LOI in the smectite-zeolite alteration zone (Franzson et al., 2008). The alteration state of the injection site rocks, estimated by LOI, is low, and increased with depth. The LOI, at the CO_2 injection depth, ranged from 0 to 8%. Unaltered primary rock content, as estimated using the Franzson

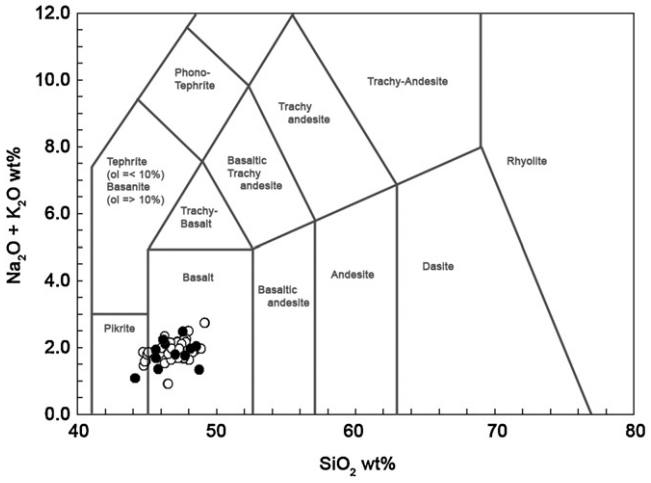

Fig. 6. A TAS diagram showing the composition of the rock at the Hellisheidi study site. The compositions of fresh and altered rocks are shown as filled and open circles, respectively. These rocks span from picrite to basalt in composition.

Table 2
Whole rock chemical analysis of drill cuttings from the CarbFix injection well HN-2, the water source HN-1 and the monitoring wells HN-4, HK-31 and HK-26.

Borehole	Vertical depth [m.a.s.l.]	Well depth [m]	Crystalline (X)/glassy (G)	Primary rock	Secondary minerals[a]	WR sample[b]	SiO_2 wt%	Al_2O_3 wt%	Fe_2O_3 t wt%	FeO[c] wt%	Fe_2O_3[c] wt%	MgO wt%	CaO wt%	Na_2O wt%	K_2O wt%	TiO_2 wt%	MnO wt%	P_2O_5 wt%	LOI %	Total %
HN-1	229.6	64	X	Picrite	–	R	48.49	14.45	13.07	10.00	1.96	8.10	12.60	1.83	0.19	1.61	0.20	0.12	−0.25	99.29
HN-1	−2.4	296	G	Basaltic tuff	Sm	R+A	47.66	13.21	15.32	11.72	2.30	6.12	9.98	1.79	0.45	2.60	0.23	0.27	2.50	98.82
HN-1	−84.4	378	G	Poorly crystalized basalt	–	R+A	47.95	13.08	16.46	12.59	2.47	6.18	10.40	2.10	0.40	2.83	0.24	0.30	0.06	98.60
HN-1	−150.4	444	X	M grained olivine tholeiite	Lim, Cc	R	47.98	15.19	12.42	9.50	1.86	7.56	11.98	1.80	0.14	1.87	0.17	0.16	1.22	99.43
HN-1	−218.4	512	X	Olivine tholeiite	Sm, Cc	R+A	46.67	14.83	12.32	9.42	1.85	8.15	12.34	1.57	0.06	1.72	0.18	0.18	1.35	98.33
HN-1	−278.4	572	X	Olivine tholeiite	Chab/Thom, Anz	R	45.66	13.95	13.70	10.48	2.06	9.38	11.08	1.58	0.09	2.04	0.20	0.22	0.96	97.69
HN-1	−292.4	586	X	Olivine tholeiite	Chab, Thom, Cc	R+A	44.99	13.69	14.28	10.92	2.14	8.92	11.22	1.73	0.09	2.20	0.21	0.22	1.77	98.11
HN-1	−472.4	766	X	Olivine tholeiite	Chab, Thom, Anz	R+A	47.46	14.53	13.38	10.23	2.01	5.76	11.76	2.00	0.18	2.24	0.19	0.20	0.93	97.49
HN-1	−608.4	902	G	Basaltic tuff	Sm, Schol/Mes	R+A	46.64	13.53	13.92	10.65	2.09	6.07	8.22	1.40	0.44	2.37	0.20	0.26	7.00	98.86
HN-1	−904.4	1198	G	Basaltic tuff	Sm, Pyr	R	46.26	13.36	14.28	10.92	2.14	6.85	10.50	1.35	0.17	2.21	0.21	0.18	3.70	97.84
HN-2	176.0	96	X+G	Olivine basalt	Heul, Qz, Lim	R+A	48.51	15.00	12.40	9.48	1.86	7.79	12.03	1.74	0.19	1.67	0.19	0.15	−0.09	98.51
HN-2	58.0	214	G	Basaltic tuff	Zeolite, Anz	R+A	45.60	12.64	14.80	11.32	2.22	6.91	9.88	1.50	0.38	2.51	0.23	0.26	4.96	98.41
HN-2	−82.0	354	G	Poorly crystalized basalt	-	R+A	46.88	13.15	15.24	11.66	2.29	6.36	11.07	1.77	0.20	2.62	0.23	0.27	1.64	98.14
HN-2	−140.0	412	X	Olivine tholeiite	Sm, Lim	R+A	48.59	14.08	13.08	10.00	1.96	6.31	12.66	1.82	0.14	1.83	0.21	0.14	0.64	98.38
HN-2	−226.0	498	X	Olivine tholeiite	Lim, Sm, Chab, Ar	R	47.61	14.87	12.10	9.25	1.82	6.94	12.01	1.65	0.12	1.56	0.18	0.12	0.91	97.03
HN-2	−314.0	586	X	Olivine tholeiite	Zeolite	R+A	45.72	15.45	11.62	8.89	1.74	6.92	11.82	1.76	0.11	1.86	0.18	0.18	4.33	98.95
HN-2	−428.0	700	X	Olivine tholeiite	Sm, Lim, Qz, Schol	R	46.99	14.24	13.03	9.97	1.95	7.31	11.82	1.64	0.17	1.90	0.19	0.15	0.98	97.30
HN-2	−576.0	848	X	Olivine tholeiite	Lim, Schol	R+A	47.21	15.11	12.51	9.57	1.88	8.48	11.58	1.56	0.12	1.69	0.18	0.11	1.85	99.33
HN-2	−648.0	920	G	Basaltic tuff	Schol, Stilb, Pyr	R+A	46.00	13.12	14.45	11.05	2.17	5.48	10.05	1.52	0.40	2.65	0.25	0.31	4.31	97.31
HN-2	−912.0	1184	G	Basaltic breccia	Lim, Schol, Stilb, Pyr	R+A	49.15	12.99	12.98	9.93	1.95	4.06	8.22	2.17	0.57	3.46	0.24	0.47	4.74	97.94
HN-4	130.5	142	G	Basaltic tuff	Qz	R	45.80	12.92	14.92	11.41	2.24	6.21	9.08	0.91	0.44	2.53	0.22	0.23	6.60	98.59
HN-4	−123.9	394	G	Basaltic tuff	Cc, Sm, Anz, Chab	R	45.72	12.57	15.30	11.70	2.30	6.33	10.45	1.60	0.34	2.61	0.23	0.27	3.87	97.97
HN-4	−210.2	500	X	Olivine tholeiite	Sm, Lim, Cc, Chal	R+A	47.61	14.98	12.55	9.60	1.88	7.25	12.69	1.58	0.09	1.60	0.19	0.12	1.43	99.02
HN-4	−290.2	596	X	Olivine tholeiite	Cc, Chab, Thom	R+A	44.93	13.88	13.10	10.02	1.97	8.58	11.42	1.51	0.08	1.92	0.20	0.20	3.60	98.29
HN-4	−364.9	700	X	Olivine tholeiite	Sm, Lim, Cc, Chab, Thom, Mes	R+A	44.71	13.91	13.88	10.62	2.08	8.64	10.91	1.77	0.09	2.26	0.22	0.18	4.11	99.50
HN-4	−433.7	802	X	Olivine basalt	Sm, Lim, Cc, Mes	R+A	47.28	14.23	13.24	10.13	1.99	7.75	12.20	1.63	0.13	1.93	0.21	0.16	1.67	99.30
HN-4	−499.7	900	X	Tholeiite	Sm, Lim, Cc	R+A	47.75	14.85	12.95	9.90	1.94	6.19	12.37	1.96	0.16	2.12	0.21	0.19	1.09	98.73
HN-4	−654.8	1130	X	Olivine basalt	Lim, Cc, Anz, Stilb, Heul	R+A	44.74	12.47	13.73	10.50	2.06	11.40	11.27	1.34	0.12	1.66	0.21	0.08	2.13	97.97
HN-4	−680.4	1168	G	Basaltic tuff	Lim, Cc, Sm, Stilb, Pyr	R+A	47.45	13.90	11.96	9.15	1.79	6.81	10.31	1.82	0.29	1.84	0.21	0.19	4.93	98.69
HK-31	179.5	102	X	Olivine tholeiite	Lim	R+A	48.87	15.03	12.46	9.53	1.87	7.84	12.36	1.78	0.18	1.65	0.19	0.15	−0.35	99.09
HK-31	43.5	238	X+G	Picrite	Lim	R+A	48.26	14.52	12.04	9.21	1.81	9.98	11.99	1.65	0.22	1.54	0.18	0.14	0.00	99.49
HK-31	−54.5	336	G	Poorly crystalized basalt	Lim	R	46.22	12.48	15.76	12.05	2.36	6.02	9.95	1.76	0.46	2.66	0.24	0.29	4.05	98.55
HK-31	−78.5	360	G	Poorly crystalized basalt	Sm, Lim, Chab, Stilb	R+A	46.27	12.71	15.72	12.02	2.36	5.99	10.15	1.88	0.46	2.67	0.24	0.30	3.05	98.09
HK-31	−154.5	436	G	Basaltic tuff	Sm, Lim	R	44.14	12.42	14.53	11.11	2.18	7.47	8.44	0.60	0.48	2.48	0.21	0.25	8.40	98.19
HK-31	−170.5	452	G	Basaltic breccia	Sm, Lim, Cc, Thom	R	46.38	11.97	19.10	14.61	2.87	4.91	10.09	1.77	0.34	3.40	0.28	0.35	0.48	97.45
HK-31	-272.5	554	G	Poorly crystalized basalt	Sm, Cc, Chab, Thom, Schol, Anz	R+A	47.23	14.34	13.05	9.98	1.96	6.92	12.17	1.70	0.16	1.84	0.20	0.15	1.88	98.52
HK-31	−298.5	580	G	Poorly crystalized basalt	Sm, Cc, Thom, Chab, Mes/Schol, Garr	R+A	45.87	15.12	12.08	9.24	1.81	7.25	12.10	1.76	0.11	1.73	0.18	0.17	3.11	98.46
HK-31	−378.5	660	G	Basaltic breccia	Sm, Cc, Thom, Chab, Mes/Schol, Garr	R+A	45.96	13.75	13.90	10.63	2.09	6.90	12.18	1.61	0.23	2.18	0.21	0.21	3.12	99.07
HK-31	−470.5	752	G	Basaltic tuff	Sm, Cc, Thom, Chab, Mes/Schol, Garr	R+A	46.50	12.85	14.79	11.31	2.22	6.30	7.86	0.61	0.30	2.03	0.22	0.16	8.01	98.37
HK-26	229.5	34	X	Olivine tholeiite	Lim	R+A	48.34	14.46	12.38	9.47	1.86	9.29	12.06	1.65	0.26	1.69	0.19	0.16	−0.30	99.12
HK-26	121.5	142	X	Olivine tholeiite	–	R	48.14	14.67	12.68	9.70	1.90	9.22	11.76	1.78	0.17	1.67	0.19	0.14	−0.43	98.90
HK-26	3.5	260	G	Basaltic tuff	Sm, Ar	R	48.74	15.14	9.71	7.43	1.46	10.98	12.75	1.20	0.13	0.71	0.17	0.03	0.32	99.06
HK-26	−128.5	392	G	Poorly crystalized basalt	Sm, Cc	R	47.60	13.23	15.97	12.21	2.40	6.09	10.62	2.13	0.36	2.73	0.24	0.31	0.15	98.06
HK-26	−218.5	482	X	Olivine tholeiite	Cc, Thom	R+A	48.01	15.40	11.42	8.73	1.71	7.72	12.96	1.50	0.13	1.40	0.18	0.10	1.15	99.00
HK-26	−420.5	684	G	Poorly crystalized basalt	Sm, Cc, Thom, Chab	R+A	46.70	12.90	14.89	11.39	2.23	6.52	10.61	1.89	0.26	2.23	0.23	0.19	3.11	98.26
HK-26	−490.5	754	G	Basaltic tuff	Sm, Cc, Thom, Chab	R+A	47.19	13.19	14.86	11.37	2.23	6.20	10.07	1.87	0.31	2.21	0.22	0.18	3.41	98.45
HK-26	−506.5	770	G	Poorly crystalized basalt	Sm, Cc, Chab, Thom, Anz	R+A	47.82	13.62	14.94	11.43	2.24	6.27	10.68	1.97	0.28	2.25	0.23	0.20	1.47	98.46
HK-26	−554.5	818	X	Olivine tholeiite	Cc, Chab, Thom, Anz	R+A	47.69	14.68	13.01	9.95	1.95	6.20	12.16	2.10	0.18	2.20	0.21	0.20	0.87	98.38
HK-26	−580.5	844	X+G	Poorly crystalized basalt	Cc, Chab, Thom, Anz	R+A	46.75	15.34	11.68	8.93	1.75	7.21	11.88	1.83	0.14	1.68	0.18	0.13	2.99	98.81

Table 2 (*Continued*)

Borehole	Well depth [m]	Zn (ppm)	Cu (ppm)	Ni (ppm)	Cr (ppm)	V (ppm)	Ba (ppm)	Sc (ppm)	Sr (ppm)	U (ppm)	Rb (ppm)	Th (ppm)	Pb (ppm)	Cr (ppm)	La (ppm)	Ce (ppm)	Nd (ppm)	Nb (ppm)	Zr (ppm)	Y (ppm)
HN-1	64	90.6	151.5	101.5	202.3	334.8	60.6	45.6	202.8	0.3	3.6	0.2	3.9	216.5	6.4	20.0	10.9	9.6	83.8	25.0
HN-1	296	132.3	229.0	60.0	63.8	415.4	138.1	46.9	207.1	0.4	8.2	0.8	2.0	76.0	16.0	44.4	26.2	26.6	179.5	39.2
HN-1	378	140.3	265.8	63.2	74.9	471.1	146.3	48.2	218.5	0.1	8.3	0.9	2.0	94.0	17.0	43.9	25.3	26.2	175.7	42.7
HN-1	444	90.8	135.1	114.0	274.0	318.6	64.7	40.5	209.6	0.0	2.7	0.1	2.1	289.2	9.1	24.7	13.9	13.3	103.8	26.7
HN-1	512	88.5	128.4	130.5	326.6	324.8	42.4	41.9	179.2	0.2	2.0	0.0	0.9	344.6	5.6	23.5	14.3	13.1	88.4	27.2
HN-1	572	101.7	149.8	185.5	400.8	344.0	48.7	38.5	194.2	0.2	1.7	0.0	3.3	429.1	7.9	24.6	17.2	14.8	101.9	29.7
HN-1	586	184.4	157.7	171.1	367.1	366.3	54.3	37.9	206.3	0.0	0.9	0.0	2.0	388.0	7.2	25.5	18.2	15.5	109.1	31.8
HN-1	766	104.7	152.7	80.1	104.3	445.3	84.3	47.9	233.7	0.1	3.1	0.0	1.5	120.0	9.5	32.6	20.2	17.1	117.6	30.4
HN-1	902	130.3	141.4	75.0	118.1	353.8	112.3	49.4	205.2	0.0	9.1	0.5	1.6	127.4	15.0	39.9	25.1	22.0	146.5	34.6
HN-1	1198	103.7	180.5	74.3	147.4	409.0	67.9	48.4	159.9	0.0	2.7	0.1	1.5	161.8	8.1	24.6	17.5	14.5	111.6	31.7
HN-2	96	91.0	141.2	108.7	346.5	335.5	76.6	43.6	189.7	0.4	2.5	0.0	1.0	367.5	9.2	25.5	14.9	13.4	100.2	26.7
HN-2	214	128.7	244.9	80.4	174.1	442.7	114.5	50.0	191.6	0.0	7.7	0.0	3.7	191.5	13.1	38.4	24.5	22.1	151.0	37.1
HN-2	354	127.1	251.3	77.1	157.2	466.2	95.4	45.4	201.6	0.6	2.6	0.0	2.8	176.5	13.0	40.6	23.7	23.3	160.3	39.8
HN-2	412	89.5	137.1	61.0	153.7	371.9	75.7	46.0	186.2	0.0	3.0	0.0	2.2	167.8	10.1	25.4	14.6	11.4	94.0	28.6
HN-2	498	93.2	147.1	97.9	306.1	335.3	59.3	47.1	180.4	0.0	1.3	0.0	2.8	321.5	5.9	20.3	11.2	9.7	80.1	24.5
HN-2	586	77.6	125.4	108.5	283.5	291.0	55.6	35.7	258.2	0.0	0.0	0.3	1.6	292.1	6.7	20.7	13.7	11.8	85.0	25.7
HN-2	700	97.6	123.1	129.5	365.7	347.7	66.6	42.0	188.4	0.1	2.8	0.0	2.0	382.5	6.6	22.1	15.2	11.5	96.2	28.6
HN-2	848	84.3	147.8	163.5	308.4	290.4	60.0	33.1	194.2	0.0	1.1	0.0	4.5	319.9	5.5	20.9	14.2	9.5	83.1	24.1
HN-2	920	139.4	121.6	66.2	114.4	339.0	107.9	46.4	205.2	0.0	9.7	0.0	1.4	122.4	15.0	42.8	26.5	23.3	158.6	39.9
HN-2	1184	147.9	57.7	28.1	37.3	356.8	172.8	46.2	197.9	0.2	9.6	2.0	2.6	46.4	23.4	64.3	39.3	35.4	243.7	61.0
HN-4	142	88.2	158.2	85.2	149.0	348.9	59.3	47.0	188.7	0.0	4.1	0.0	2.6	160.6	5.2	18.4	10.9	9.4	81.4	25.1
HN-4	394	134.2	254.5	84.0	186.9	353.6	116.8	52.6	208.4	0.0	13.7	0.0	0.8	204.7	12.0	36.1	24.1	22.0	150.7	37.3
HN-4	500	95.1	132.2	236.8	751.5	306.9	79.8	44.6	187.4	0.5	5.8	1.0	1.2	773.5	7.2	23.7	14.0	15.4	94.5	22.7
HN-4	596	135.6	260.8	81.6	179.5	463.4	114.5	52.0	182.5	0.1	6.6	0.0	1.7	194.7	11.8	42.6	25.5	22.9	157.3	39.0
HN-4	700	96.7	132.9	172.3	315.4	320.3	42.4	35.3	198.0	0.2	0.6	0.0	1.0	330.8	6.0	22.4	14.1	13.2	88.1	27.4
HN-4	802	104.9	137.8	177.4	358.8	328.9	63.8	34.2	250.8	0.0	0.6	0.0	3.0	377.8	6.3	21.4	14.9	12.7	94.1	27.5
HN-4	900	100.0	137.2	138.7	356.1	361.6	58.3	43.1	180.3	0.2	1.5	0.0	1.3	381.6	5.6	24.1	15.2	11.2	93.4	28.8
HN-4	1130	99.4	146.1	81.8	172.8	396.2	75.3	46.4	224.2	0.1	2.8	0.6	2.6	185.1	10.2	27.6	18.1	15.3	109.1	29.1
HN-4	1168	97.1	102.6	246.8	581.7	334.8	43.7	40.8	153.5	0.0	1.8	0.0	2.7	610.4	3.0	13.6	10.4	7.7	65.8	20.0
HK-31	102	89.6	148.2	107.6	359.5	338.6	70.3	42.9	186.5	0.3	3.8	0.6	2.6	373.6	7.6	23.6	15.6	13.1	98.7	26.9
HK-31	238	140.1	244.2	61.8	48.1	429.2	146.7	48.4	213.4	0.3	9.0	0.4	2.5	65.1	19.4	46.8	26.0	26.5	181.4	39.4
HK-31	336	85.1	123.8	186.8	590.8	306.6	80.7	40.7	196.2	0.3	3.0	0.4	1.9	607.1	7.5	23.2	13.3	13.3	89.6	23.9
HK-31	360	140.2	244.1	65.1	56.7	439.8	153.0	47.2	212.2	0.2	9.0	0.5	1.5	73.2	17.6	46.7	26.0	26.5	178.1	40.1
HK-31	436	134.1	258.8	79.1	173.0	439.9	123.9	52.4	263.2	0.0	8.0	0.7	1.0	183.7	12.1	38.9	25.6	21.0	143.8	35.2
HK-31	452	168.5	345.3	54.5	50.2	525.7	124.2	48.1	199.0	0.0	8.1	0.5	2.3	68.4	14.2	47.4	31.4	28.9	203.5	51.5
HK-31	554	99.9	172.2	84.2	235.2	349.9	65.0	43.3	187.2	0.3	2.0	0.0	1.5	247.9	7.4	25.2	14.8	12.6	98.8	28.4
HK-31	580	90.1	357.0	121.5	263.0	298.5	57.3	35.6	213.7	0.0	2.6	0.7	12.6	274.2	7.7	22.3	16.0	13.1	91.0	26.4
HK-31	660	114.1	196.3	103.6	219.7	365.8	97.3	40.7	255.3	0.1	4.5	0.0	2.6	240.0	9.9	33.2	19.8	17.6	124.8	33.1
HK-31	752	122.3	169.7	75.8	81.4	303.0	78.7	50.6	140.4	0.0	10.9	0.0	0.9	96.0	9.2	29.4	16.7	14.7	105.5	28.0
HK-26	34	85.1	129.4	171.9	551.5	331.4	99.7	43.7	216.4	0.3	4.6	1.2	20.3	570.6	10.5	26.0	15.6	16.5	103.7	24.6
HK-26	142	96.7	145.4	160.4	401.9	329.7	72.9	40.9	195.2	0.8	2.9	0.0	11.7	418.0	7.6	24.4	14.3	12.2	98.1	26.3
HK-26	260	66.9	117.5	229.4	688.6	242.1	43.9	46.6	97.0	0.0	4.2	0.3	7.7	713.4	3.3	9.4	4.4	4.8	36.5	17.1
HK-26	392	136.7	242.3	61.5	44.2	455.0	126.7	46.2	230.3	0.5	7.2	0.5	4.3	61.9	16.4	45.3	28.3	28.0	191.0	41.9
HK-26	482	77.1	110.2	118.5	296.2	283.4	58.3	38.5	206.4	0.0	2.0	0.9	1.0	307.1	7.1	21.1	10.6	8.7	74.6	22.2
HK-26	684	122.2	175.5	60.9	52.6	412.8	85.8	51.1	206.5	0.3	5.9	0.0	1.8	65.7	12.1	32.0	18.9	16.9	121.7	32.5
HK-26	754	122.1	174.2	61.1	52.9	376.2	96.5	51.5	215.5	0.3	6.9	0.0	1.0	63.2	9.4	30.5	19.7	16.7	120.1	31.7
HK-26	770	121.2	172.8	59.9	50.4	405.7	108.2	48.4	217.1	0.1	7.1	0.0	1.6	63.3	10.2	30.9	19.7	17.3	123.4	33.0
HK-26	818	100.2	141.4	68.6	105.0	400.2	92.9	45.1	242.2	0.3	1.5	0.3	0.9	117.5	9.3	27.9	19.6	16.8	116.2	30.0
HK-26	844	86.4	120.0	134.1	295.7	305.8	70.3	37.4	230.5	0.0	1.1	0.8	0.4	312.9	7.7	20.3	14.2	11.3	86.3	23.6

[a] Secondary minerals observed in the drill cuttings: Sm = Smectite, Lim = Limonite, Cc = Calcite, Ar = Aragonite, Thom = Thomsonite, Chab = Chabazite, Anz = Analzime, Schol = Scholesite, Mes = Mesolite, Garr = Garronite, Stilb = Stilbite, Heul = Heulandite, Pyr = Pyrite, Qz = Quartz.

[b] The samples for the WR chemical analysis consisted either of primary rock with alteration (R + A) or only primary rock (R).

[c] FeO and Fe_2O_3 calculated assuming 85% FeO and 15% Fe_2O_3.

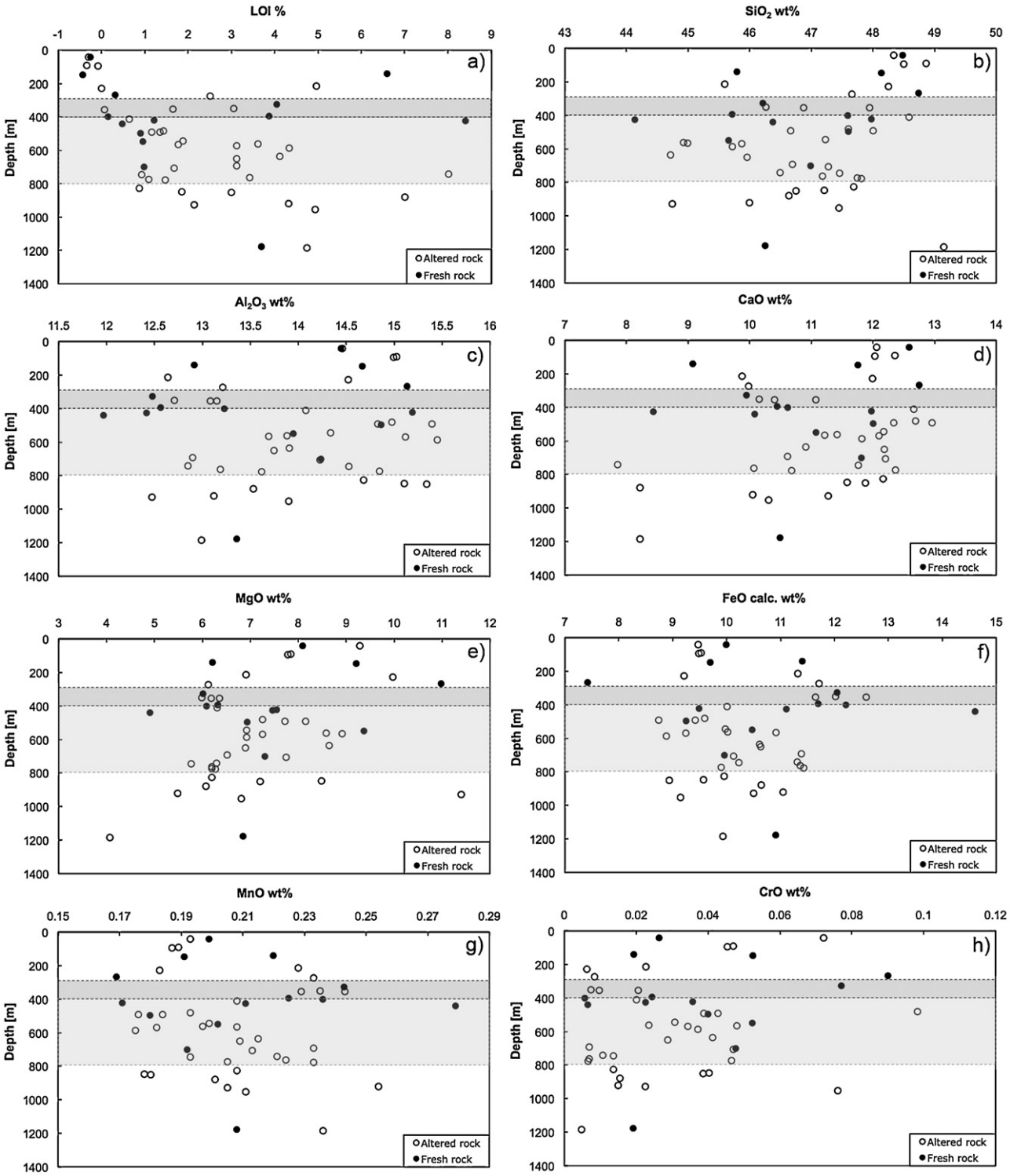

Fig. 7. Chemical composition of the rocks as a function of depth in wells HN-1, HN-2, HN-4, HK-31, and HK-26. (a) Loss on ignition, (b) Silica, (c) Aluminum, (d) Calcium, (e) Magnesium, (f) Iron (II), (g) Manganese, and (h) Chromium. All numbers are given in wt%. The filled circles represent "fresh" rocks and the open circles altered rocks (see Section 3.3). The dark gray shaded area represents the depth of the upper hyaloclastite rock formation (see Fig. 4) and the light-gray shaded area is the target CO_2 injection zone.

et al. (2008) LOI correlation, is shown for various depths in Fig. 8a. The primary rock content was highest in the shallow lava flows; 80–90% of these rocks are primary. The primary rock content of the hyaloclastite at this depth is substantially lower. At 400–800 m depth the majority of the lava flows contain over 80% primary material; the majority of the hyaloclastite contained 40–80% of primary rocks at this depth.

Fig. 8b shows the moles of divalent cations per kilogram of basalt, measured in the rocks collected from HN-2 and HN-4, from 400 to 800 m depth. These rocks contain between 5 and 6 moles of divalent cations/kg and Ca, Mg, and Fe are the dominant contributors. If the redox dependent cations are excluded, the rocks will release ~4 moles of divalent cations/kg basalt if it is dissolved completely. The concentration of dissolved inorganic carbon

Table 3
Example of water chemical analysis of the CarbFix injection well HN-2, the water source HN-1 and monitoring wells HN-4, HK-34, HK-31, HK26, HK-13, HK-7B, HK-12, and HK-25 (see electronic supplement for all data).

Borehole	Sample	Sampling date dd.mm.yy	*T* °C (*in situ*)	pH/*T* °C	Cond. (*in situ*) (μS/cm)	H_2S (titr.) (μmole/L)	O_2 (titr.) (mmol/L)	Alk. (titr.) (meq./kg)	DIC (IC) (mmol/L)	DOC (mmol/L)
HN-1	08HAA02	01.07.08	19.0	8.87/19.0	212/19.0	–[b]	0.057	1.91	1.815	0.026
HN-2	09HAA16[a]	19.05.09	15.5	8.79/22.3	342/15.5	1.300	0.011	1.45	1.267	0.137
HN-4	08HAA01	01.07.08	32.3	9.43/18.8	220/32.3	–	0.037	1.91	1.464	0.022
HK-34	08HAA03	04.07.08	25.0	9.63/21.8	215/25.0	–	0.015	1.98	1.414	0.145
HK-31	08HAA05	04.07.08	17.4	9.29/21.8	229/17.4	–	0.015	1.92	1.659	0.031
HK-26	08HAA06	04.07.08	18.8	8.44/21.8	381/18.8	–	0.011	3.78	3.660	0.022
HK-13	08HAA07	08.07.08	9.1	7.44/23.6	90/9.1	–	0.380	0.39	0.396	0.040
HK-7B	08HAA08	08.07.08	12.4	7.65/23.6	156/12.4	–	0.281	0.85	0.871	0.024
HK-12	08HAA04	04.07.08	8.0	8.24/21.8	121.6/8.0	–	0.393	0.72	0.732	0.039
HK-25	08HAA09	08.07.08	8.9	7.96/21.3	119.4/8.9	–	0.358	0.66	0.663	0.042

Borehole	F (IC) (mmol/L)	Cl (IC) (mmol/L)	SO4 (IC) (mmol/L)	Cl ICP-MS) (mmol/L)	S (t) (ICP-MS) (mmol/L)	Si ICP-MS) (mmol/L)	Na ICP-MS) (mmol/L)	K ICP-MS) (mmol/L)	Ca ICP-MS) (mmol/L)	Mg ICP-MS) (mmol/L)	Fe (ICP-MS) (μmole/L)
HN-1	0.014	0.247	0.075	0.247	0.085	0.363	1.301	0.027	0.164	0.313	0.016
HN-2	0.013	0.222	0.077	0.238	0.088	0.337	1.338	0.012	0.124	0.149	0.399
HN-4	0.026	0.228	0.089	0.228	0.102	0.897	2.114	0.019	0.041	0.005	0.064
HK-34	0.020	0.231	0.079	0.231	0.095	0.812	2.157	0.017	0.054	0.009	0.138
HK-31	0.038	0.230	0.095	0.230	0.114	0.741	1.818	0.057	0.094	0.028	0.098
HK-26	0.035	0.262	0.137	0.262	0.154	0.637	3.154	0.154	0.143	0.274	0.874
HK-13	0.000	0.295	0.036	0.295	0.035	0.321	0.279	0.022	0.117	0.117	0.097
HK-7B	0.008	0.261	0.172	0.261	0.185	0.427	0.399	0.025	0.282	0.246	0.048
HK-12	0.008	0.253	0.068	0.253	0.080	0.321	0.364	0.022	0.214	0.176	0.064
HK-25	0.008	0.305	0.061	0.305	0.067	0.346	0.331	0.025	0.198	0.186	0.184

Borehole	Sample	Al ICP-MS) (μmole/L)	Sr ICP-MS) (μmole/L)	Mn ICP-MS) (μmole/L)	Ti ICP-MS) (μmole/L)	P ICP-MS) (μmole/L)	Mo ICP-MS) (μmole/L)	B CP-MS) (μmole/L)	As (ICP-MS) (μmole/L)	Cr (ICP-MS) (μmole/L)
HN-1	08HAA02	0.419	0.264	0.062	0.001	1.359	0.010	0.897	0.005392	0.001962
HN-2	09HAA16[a]	0.097	0.140	0.096	< 0.01	0.680	< 0.14	0.888	–	–
HN-4	08HAA01	1.905	0.018	0.024	0.002	0.268	0.024	2.100	0.0125	<0.0002
HK-34	08HAA03	1.286	0.045	0.032	0.006	0.345	0.022	1.720	0.0107	0.0004
HK-31	08HAA05	1.979	0.136	0.059	0.002	0.717	0.028	2.599	0.0094	0.0007
HK-26	08HAA06	0.486	0.323	0.288	0.001	1.069	0.041	4.643	0.0029	<0.0002
HK-13	08HAA07	0.102	0.135	0.011	0.002	0.429	0.001	0.604	<0.0008	0.0039
HK-7B	08HAA08	0.057	0.229	0.006	0.000	1.279	0.006	0.671	<0.0008	0.0145
HK-12	08HAA04	0.203	0.170	0.011	<0.00002	0.914	0.006	0.403	<0.0009	0.0194
HK-25	08HAA09	0.135	0.153	0.030	0.001	0.823	0.002	0.376	<0.0009	0.0103

Borehole	Ba (ICP-MS) (μmole/L)	V (ICP-MS) (μmole/L)	Co (ICP-MS) (μmole/L)	Cu (ICP-MS) (μmole/L)	Ni (ICP-MS) (μmole/L)	Pb (ICP-MS) (μmole/L)	Zn (ICP-MS) (μmole/L)	Ce (ICP-MS) (μmole/L)	N (t) (IC) (μmole/L)	NH_4 (Aan) (μmole/L)	NO_3 (IC) (μmole/L)
HN-1	0.004391	0.288566	<0.00008	<0.0016	0.009984	0.000070	0.003669	<0.000007	4.594	0.892	0.758
HN-2	–	–	–	–	–	–	–	–	–	–	–
HN-4	0.0006	0.1213	0.000173	0.001810	0.008468	0.000106	0.003134	0.000009	3.756	1.966	0.184
HK-34	0.0019	0.1930	0.000273	0.001621	0.009183	<0.00005	0.005840	0.000009	3.277	0.572	0.039
HK-31	0.0087	0.2886	<0.00008	<0.0016	0.007957	<0.00005	<0.003	<0.000007	8.565	0.915	<0.145
HK-26	0.0450	0.0088	0.000134	<0.0016	0.006730	0.000070	<0.003	0.000010	3.456	0.663	<0.145
HK-13	0.0034	0.1142	0.001581	0.002691	0.006764	0.000147	3.929123	<0.000007	6.895	1.143	3.697
HK-7B	0.0017	0.3965	0.000192	0.004107	0.009337	<0.00005	0.056567	<0.000007	9.065	0.412	6.094
HK-12	0.0060	0.3592	0.000299	0.002345	0.010325	<0.00005	0.023544	<0.000007	7.018	1.555	3.620
HK-25	0.0057	0.2140	0.000185	<0.0016	0.006372	<0.00005	0.065434	<0.000007	8.055	1.032	4.657

[a] Analyzed at IES.
[b] Not analyzed.

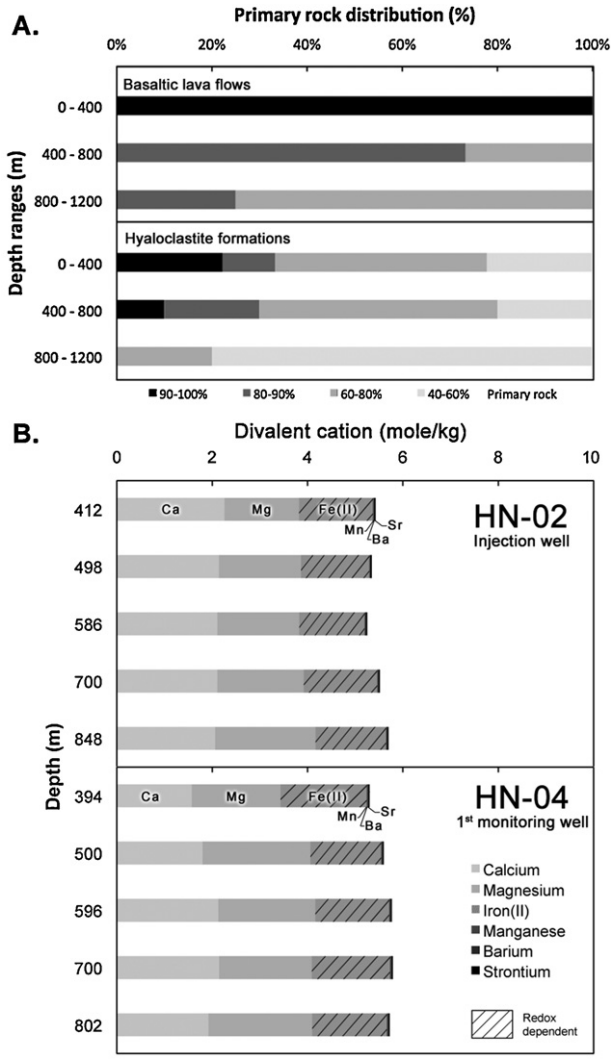

Fig. 8. (a) Distribution of calculated unaltered primary rock content of the lava flows and the hyaloclastites at the study site at selected depths. (b) Divalent cations concentrations in mole/kg rock in the basaltic rocks of our study site at depths between 400 and 800 m in the HN-2 injection well and HN-4 monitoring well.

in the injection water at 20° C and 25 bar pressure of CO_2 will be ~1 mole/kg (Gislason et al., 2010). Fig. 8b suggests that about 170–200 g of basalt are needed to fix the carbon in 1 kg of injection water, assuming that all divalent cations eventually form carbonate minerals.

4.3. Water chemistry

Water samples were collected from 9 wells at the injection site every two months from July 2008 to November 2010. Temperature, dissolved H_2S, O_2, organic carbon, pH, alkalinity and total dissolved inorganic carbon (DIC) were measured as well as the concentration of 30–50 dissolved inorganic major and trace elements. Measured water compositions are provided in Table 3 and the Electronic Supplement. The concentration of selected elements and water temperature of these samples is shown in Fig. 9.

The groundwater system is divided into upper- and lower parts, separated by the low-permeable upper hyaloclastite formation shown in Fig. 4 (Aradóttir et al., 2011). The shallow wells, HK-7b, HK-12, HK-13, and HK-25, draw water from the dominate aquifers in the upper system, whereas the deeper wells, HN-2, HN-4, HK-34,

Table 4
The dissolved gas composition of HN-2 injection fluids: HN-1 water equilibrated pure CO_2 and 75% CO_2, 24.2% H_2S and 0.8% H_2 at 25 bar pressure and 25° C.

Injected gas	pH	pε	Aqueous phase concentration				Aqueous phase partial pressure		
			$CO_{2(aq)}$ (mmol/L)	$H_2S_{(aq)}$ (mmol/L)	SO_4 (mmol/L)	$O_{2\,(aq)}$ (mmol/L)	pCO_2 (bar)	pH_2S (bar)	P_{tot} (bar)
Pure CO_2	3.74	16.60	830.0	0.00	0.13000	0.06	25.0	0.0	25.0
75% CO_2, 24.2% H_2S, 0.8% H_2	4.03	−0.67	418.0	135	0.00054	0.00	12.6	1.4	14.0

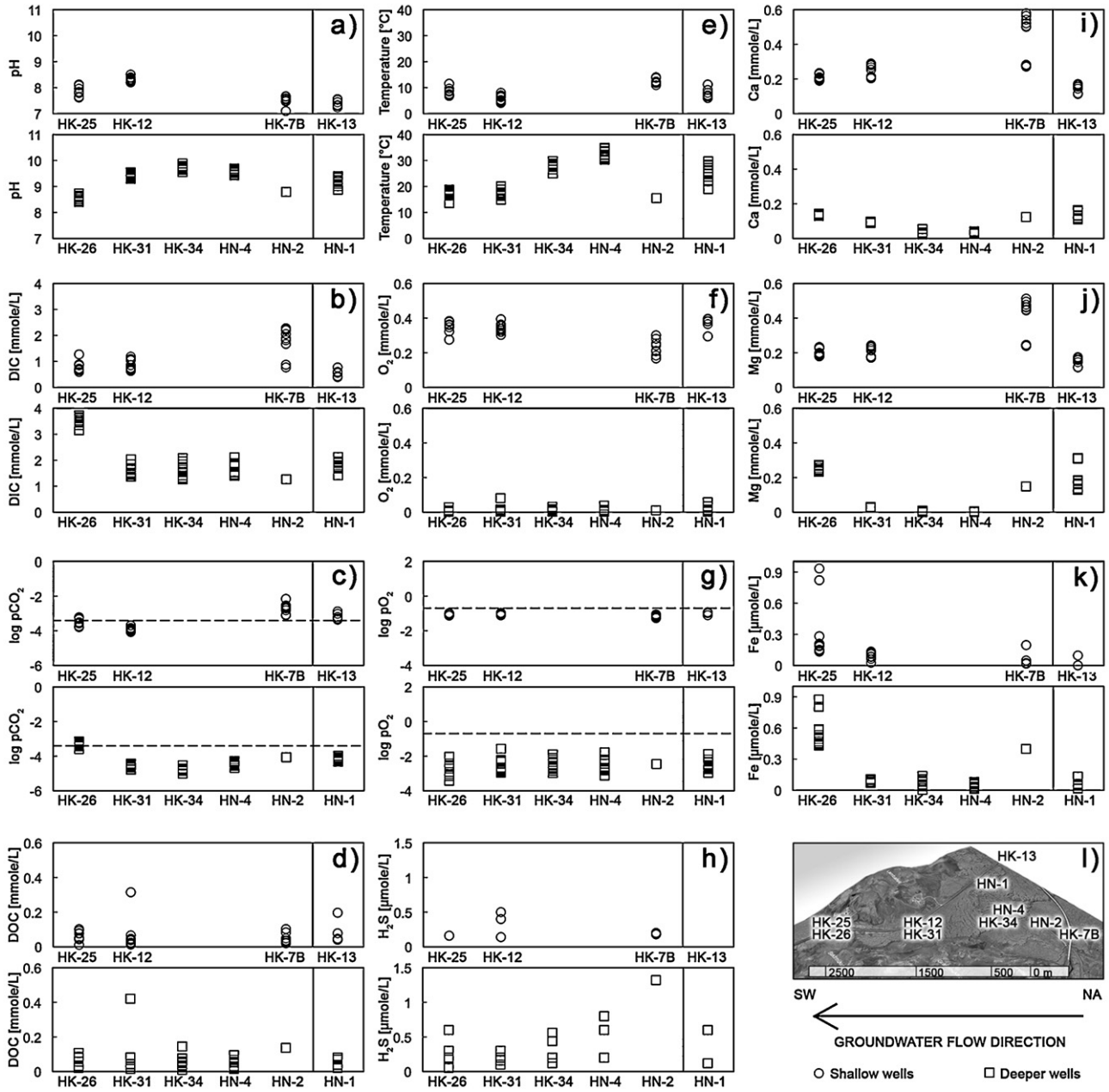

Fig. 9. Spatial distribution of selected dissolved compounds in the upper and lower groundwater systems at the study site. (a) pH, (b) dissolved inorganic carbon, (c) log pCO_2, (d) dissolved organic carbon, (e) temperature, (f) dissolved oxygen, (g) log pO_2, (h) dissolved hydrogen sulphate, (i) Calcium, (j) Magnesium, and (k) Iron. (l) Aerial photograph showing the spatial distribution of the groundwater wells and groundwater flow direction.

HN-1, HK-31, and HK-26, draw water from the highest discharge aquifers below 400 m since these wells are cased down to that depth. There is just one sample available from the HN-2 injection well. The HN-1 well is the water source for the injection. Water from this well was colder and higher in dissolved oxygen content than the water from the other deep monitoring wells at the beginning of the study period. Well HN-1 might have drawn water from the upper ground water system during intensive pumping (40–70 kg/s) to service drill rigs during 2007–2008.

The temperatures of the water drawn from the deeper wells, ranged from 15 to 35 °C. It was highest in water from the monitoring well HN-4 closest to the injection well, and dropped to 17–20 °C downstream toward the south west (see Fig. 9). The lowest temperature was measured in the injection well HN-2, possibly due to insufficient pumping prior to sampling. The *in situ* pH ranged from 8.9–9.8 in all the wells, except for HK-26, the well furthest south, where it was 8.4–8.8. This well also exhibited higher dissolved inorganic carbon (DIC) than the other deeper wells. Calculated *in situ* pCO_2 showed the same trend; all of the deeper wells were undersaturated with respect to atmospheric pCO_2, except for HK-26, which was slightly oversaturated. Dissolved organic carbon (DOC) was similar in all the wells, ranging mainly from 0.01 to 0.1 mmol/L.

Measured pH and temperature were lower in the shallow wells. The *in situ* pH ranged from 7.2 to 8.7 and temperatures varied from 8 to 12 °C (see Fig. 9). The DIC varied from 0.4 to 1.2 in the shallow wells except for HK-7b, which showed sudden increase in DIC, Ca, Mg, Fe, and Sr in the spring of 2009. The shallow groundwater system was close to saturation with respect to atmospheric O_2. The deeper system was undersaturated, ranging from 0 to

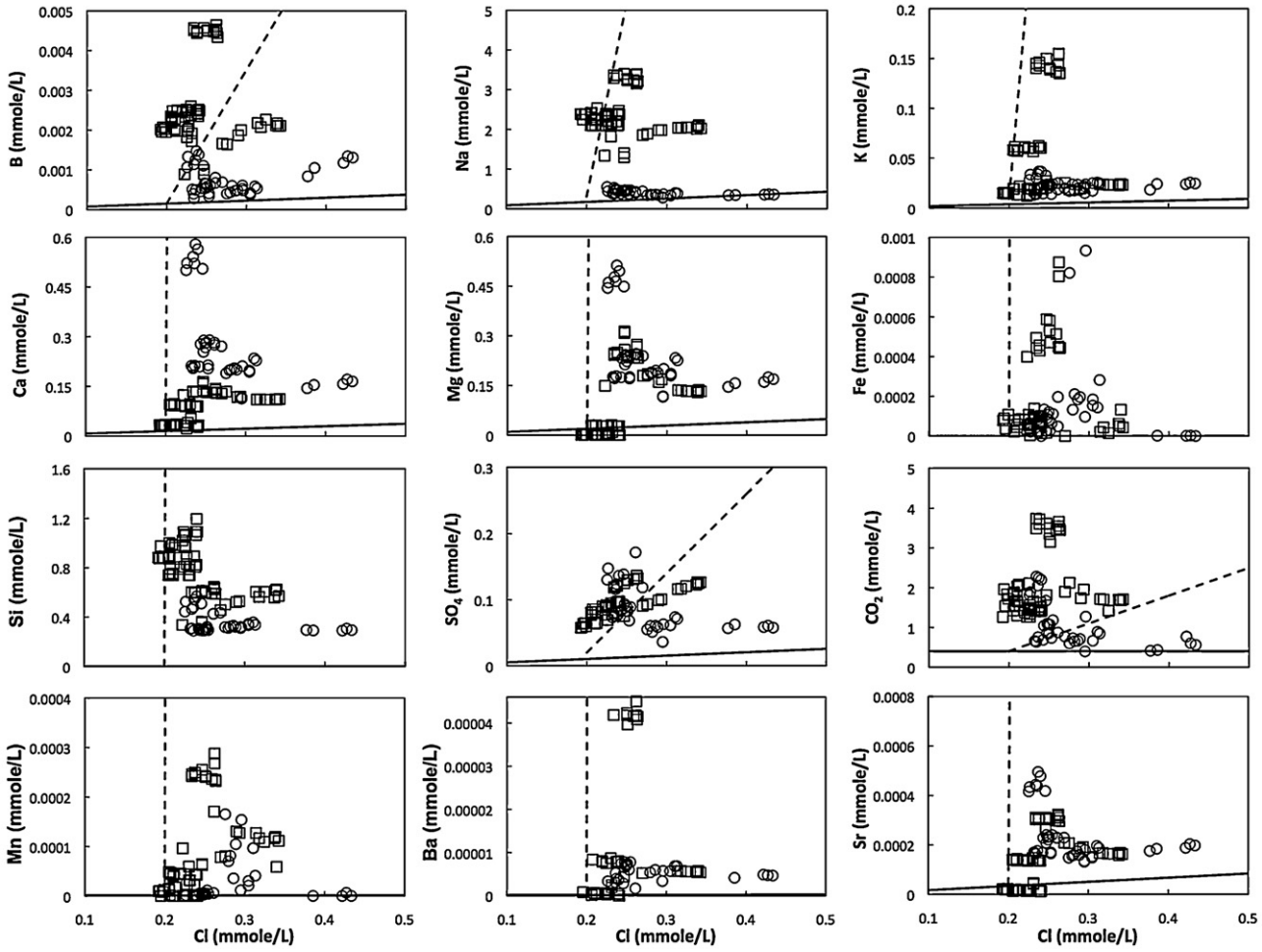

Fig. 10. Aqueous concentration of selected elements as a function of the corresponding chlorine concentration. The slope of the dashed line equals the element ratio of these elements in the basalt (see Section 3). The solid line represents the seawater ratio of these elements. The symbol shape indicates the depth of the sample wells; squares depict the composition of the deep monitoring wells and the circles show the composition of the shallow monitoring wells. The seawater ratios for Si/Cl, Mn/Cl, Ba/Cl, and Fe/Cl are indistinguishable from the horizontal axes.

0.08 mmol/L. The H_2S was barely detectable in the all samples; the deeper aquifer system contained slightly higher values, ranging from 0 to 1.4 μmol/L. The concentration of Ca and Mg was higher in the upper groundwater system than in the lower system but Fe concentrations were similar. These observations suggest that the upper groundwater system is in communication with atmospheric CO_2 and O_2, but the lower system is isolated from the atmosphere (Gislason and Eugster, 1987a, 1987b; Gislason and Arnórsson, 1990; Arnórsson et al., 2000). The decrease in the partial pressure of O_2 and CO_2, and the Ca and Mg concentrations with depth suggests their consumption by secondary minerals. The low Fe concentration suggests its consumption by secondary minerals in both the upper and lower systems.

Chlorine and boron concentrations have been used to monitor reaction progress during water/basalt interactions, and to correct for the seawater-derived rainwater contribution to natural waters (Gislason and Eugster, 1987a; Arnórsson and Andrésdóttir, 1995; and Eiriksdottir et al., 2008). Both elements are assumed to be conservative and mobile, that is to say, they are not consumed by secondary minerals after their release from primary minerals and glass. The variation of various element concentrations *versus* that of chlorine is shown in Fig. 10. When rainwater circulates through basalts, its chemistry is controlled by the initial concentration and water-rock interaction. Seawater derived Cl concentration in rainwater decreases with increasing elevation and distance from the ocean (Sigurdsson and Einarsson, 1988). The initial Cl concentration of the deeper system is lower than the upper system, suggesting its source is further inland. Because the elevation of the study area is 260–290 m.a.s.l., the deeper system is more than 100 m below sea level. Nevertheless, the low dissolved Cl concentration of the deeper system suggests that its water originated from mountains located a few kilometers northeast of the injection site, rather than from seawater infiltration (Sigurdsson and Einarsson, 1988). This conclusion is in agreement with studies of ^{18}O and deuterium of waters derived from hot and cold wells in the Hengill geothermal system (Mutonga et al., 2010).

In the shallow groundwater system, elements like B, Na, K, and Cl exhibited close to the seawater ratios, reflecting limited water/rock interactions. Deeper in the system where the waters had traveled further, B/Cl, Na/Cl and sometimes K/Cl concentration ratios increase relative to that of seawater. Boron, Na, and K can be derived from rock dissolution, are mobile, and are not consumed significantly by secondary minerals. Calcium/Cl, Mg/Cl, and Sr/Cl concentration ratios exhibited an opposite trend; these ratios decreased with depth as Ca, Mg, and Sr were consumed by calcite, Ca-rich zeolites, and clay mineral precipitation in the deeper groundwater system (see Figs. 4, 5 and 10). Other metal/chloride ratios, *i.e.* Si, Fe, Ba, and Mn showed slight increases with depth,

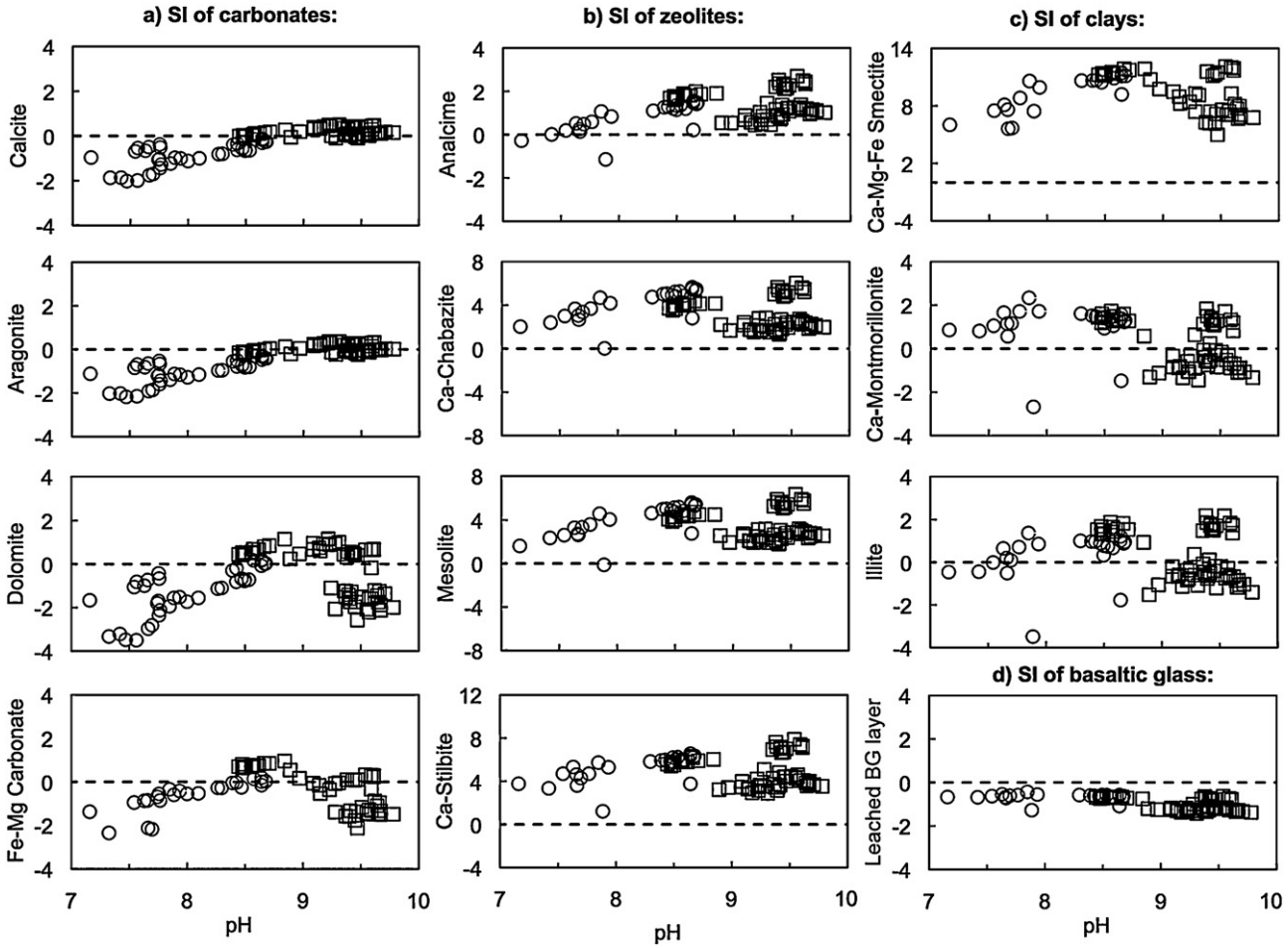

Fig. 11. Saturation indices of selected primary and secondary phases as a function of pH of the sampled well waters. (a) Carbonates, (b) Zeolites, (c) Clays and (d) Hydrated basaltic glass (leached basaltic glass). Circles represent the saturation states of shallow ground water and the squares represent the saturation states of the deeper ground water.

yet were also consumed by clays, zeolites and carbonates. The SO_4/Cl concentration ratio was similar in both systems suggesting some consumption by sulphide minerals in the lower system. The CO_2 content of the waters suggests that some deep external CO_2 entered the deeper waters and the shallow well water of HK-7b. The relative mobility of elements during water-basalt interaction, before CO_2-injection at the Hellisheidi site, is described in Appendix A – Supplementary data.

5. Geochemical modeling

5.1. Saturation indices for secondary minerals

PHREEQC was used to calculate the *in situ* chemical speciation of the well waters, and the saturation state of these waters with respect to gases, and primary and secondary minerals. The average charge balance error was 2.4% for the 102 samples with standard deviation of 1.88.

The calculated saturation index for various minerals is shown as a function of *in situ* pH in Fig. 11. The water in the deep wells was saturated with respect to calcite and aragonite, and close to saturation with respect to Fe-Mg carbonates. They were supersaturated with respect to calcium rich zeolites and clays including heulandite, stilbite, mesolite, chabazite, and smectite. The water from the shallow wells showed similar results, but were mostly undersaturated with respect to calcite and Fe–Mg carbonates. All of the samples were undersaturated with respect to leached basaltic glass ($SiAl_{0.35}O_2(OH)_{1.05}$). These results are consistent with the observed spatial distribution of the secondary minerals found in the drill cuttings of the boreholes (Figs. 4 and 5).

5.2. Water- gas equilibration within the injection well HN-2

Calculations were performed to simulate the chemistry of gas charged injection water at the Hellisheidi site. Two gas compositions were considered: (i) 100% CO_2 and (ii) 75% CO_2, 24.2% H_2S and 0.8% H_2. These gases were dissolved into HN-1 water (see Table 3 for chemical composition) at 25 °C and 25 bar injection pressure, mimicing injection conditions. Note that reservoir temperature in the main aquifers of the first monitoring wells, HN-4 and HK-34, are slightly higher ~30 °C and ~27 °C, respectively; but decreases downstream towards south (see Table 3 and Electronic Supplement). These slight temperature variations were not included in the model calculations. The injected gas pressure was 25 bar, and the hydrostatic pressure increases from 25 to 40 bar as gas and water desend during injection. This pressure increase is not considered in the calculations, since the partial pressure of the gases injected matters the most in the thermodynamic calculations. Furthermore, these calculations were done assuming the partial pressures of CO_2, H_2S and H_2 to be equal of the gas fugacities. This can result in slight over estimation of the dissolved gas consentrations at the respective partial pressures of the individual gases (≤25 bar).

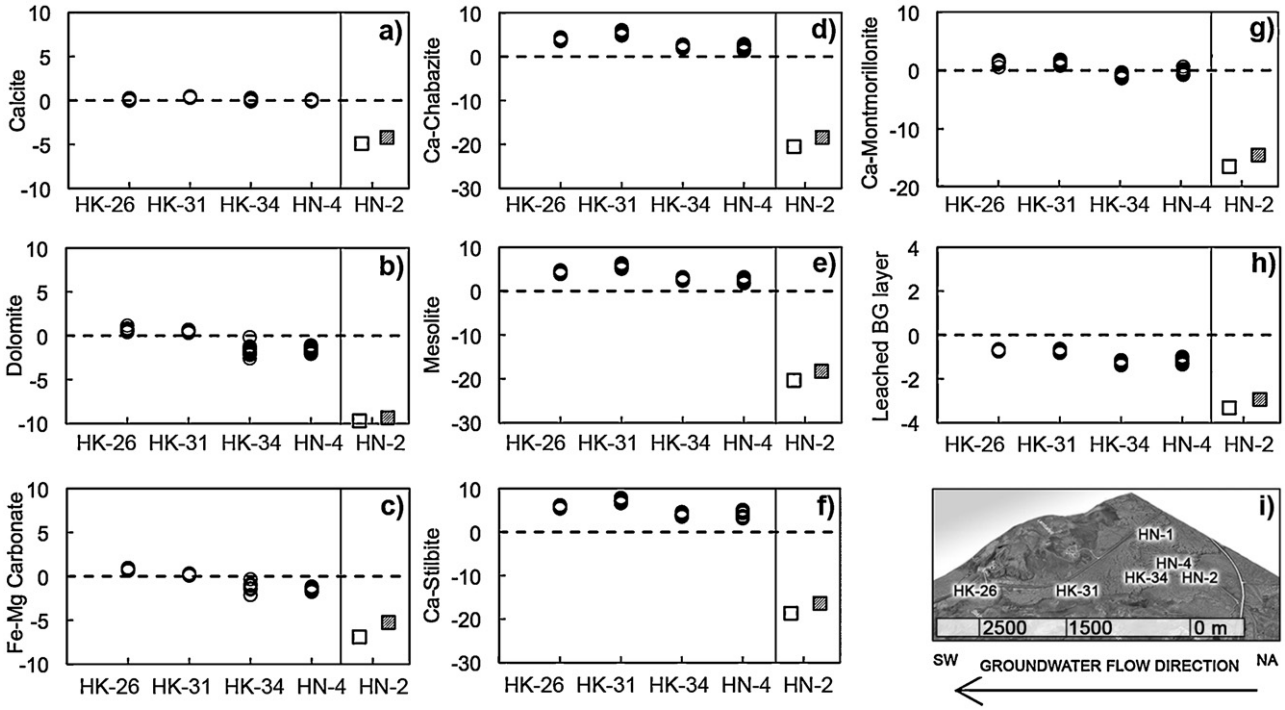

Fig. 12. Spatial distribution of saturation indices in the pre-injection deep groundwaters for several primary and secondary phases (circles) and those predicted in HN-2 during gas equilibration calculations. The white and gray squares correspond to calculations performed using aqueous fluids equilibrated with pure CO_2 and CO_2–H_2S–H_2 gas mixture equilibrated fluid, respectively, at 25 bars of pressure and 25 °C: (a) Calcite, (b) Dolomite, (c) Fe–Mg Carbonate, (d) Ca-Chabazite, (e) Mesolite, (f) Ca-Stilbite, (g) Ca-Montmorillonite, (h) Basaltic glass (leached BG layer). (i) Spatial distribution of the wells and groundwater flow direction shown on this areal photograph.

The resulting compostions of these fluids is summarized in Table 4. The $CO_{2\ (aq)}$ and $H_2S_{\ (aq)}$ concentrations, and pH of the resulting fluids are 835 mmol/L, 0.00 mmol/L, and 3.74, and 418 mmol/L, 135 mmol/L, and 4.03, respectively for the HN-1 water equilibrated with pure CO_2 and 75% CO_2 + 24.2% H_2S + 0.8% H_2, respectively. The equilibrium gas partial pressure CO_2 and H_2S is relatively low for the HN-1 water equilibrated with the 75% CO_2 + 24.2% H_2S + 0.8% H_2 gas mixture, owing to the low solubility of H_2. The addition of the H_2, however, changes the redox state of the fluid phase, preventing most H_2S oxidation.

The saturation indices for selected secondary minerals and leached basaltic glass in HN-1 water, after its equilibration with the gases, are shown in Fig. 12. The addition of CO_2 and H_2S lowers dramatically the saturation state of the water with respect to all the primary and secondary phases that are present in the host rocks at the study site.

5.3. Reaction path modeling

One liter of these gas-saturated injection fluids were used in further PHREEQC calculations to assess their interaction with Stapafell basaltic glass (*e.g.* Oelkers and Gislason, 2001; Gislason and Oelkers, 2003; Gysi and Stefánsson, 2011). Basaltic glass represents the glassy tops and bottoms of the lava flows at the Hellisheidi site. Furthermore, by choosing single phase primary rock, the simulations were simplified to overcome the differencials, and in some cases unknown, dissolution rates of the multiphase crystalline basalts. Selected secondary minerals found associated with low temperature (<100 °C) CO_2–H_2S–water–basalt interaction (Benning et al., 2000; Rogers et al., 2006; Hunger and Benning, 2007; Gysi and Stefánsson, 2011; Stefánsson et al., 2011) were allowed to precipitate, if saturated in the aqueous phases. For example, quartz was not allowed to precipitate, although more stable than calcedony. The results of these calculations can be seen in Figs. 13 and 14.

In the pure CO_2 injection the dissolution of 1 to 1.8 moles of basaltic glass[1] was needed to raise the pH to 8–9, the pH in the field prior to injection (Figs. 9, 13 and 14). The redox state, depicted as pε in Fig. 14, was calculated based on the oxygen concentration for the injected fluid phase. As the basaltic glass dissolved in this fluid, the dissolved FeII/FeIII redox couple was used to fix pε. The first carbonate minerals calculated to form were Ca–Mg–Fe–carbonate and dolomite at pH less than 7–8. Ankerite ($CaFe(CO_3)_2$) is calculated to precipitate between pH 8 and 9, and finally calcite at pH > 9. Chalcedony and kaolinite precipitated throughout the model calculations. Iron hydroxide precipitated at pH 3.7–7. The main clay minerals formed were Mg-smectite, Ca–Mg–Fe–smectite, and celadonite at pH above 6.

The 75% CO_2 + 24.2% H_2S + 0.8% H_2 gas mixture injection model showed the similar trends; results are shown in Figs. 13 and 14b. The evolution of this fluid does, however exhibit several significant differences from that of the pure CO_2 injection. First, owing to the presence of H_2, this fluid is more reducing. Second, less than 0.7 moles of basaltic glass were needed to raise pH to its pre-injection value. The hydrogen sulfide precipitated as elemental sulfur early in the model calculation but as greigite and later mackinawite with increasing basaltic glass dissolution. The sulfur was fully sequestered after less than 0.5 moles of basaltic glass had dissolved as shown in Fig. 13f. In this calculation, CO_2 was mostly seqestered at low pH as dolomite and to a lesser degree as Ca-Mg-Fe-carbonate, changing into ankerite at around pH 9 and finally calcite above pH 9. Chalcedony and kaolinite precipitated throughout the simulations. Mg-smectite and celadonite precipitated above pH 6. At pH > 8 Ca–Mg–Fe–smectite, and the zeolites analcime and scolecite formed.

[1] A mole of basaltic glass is defined based on each mole of glass containing one mole of Si.

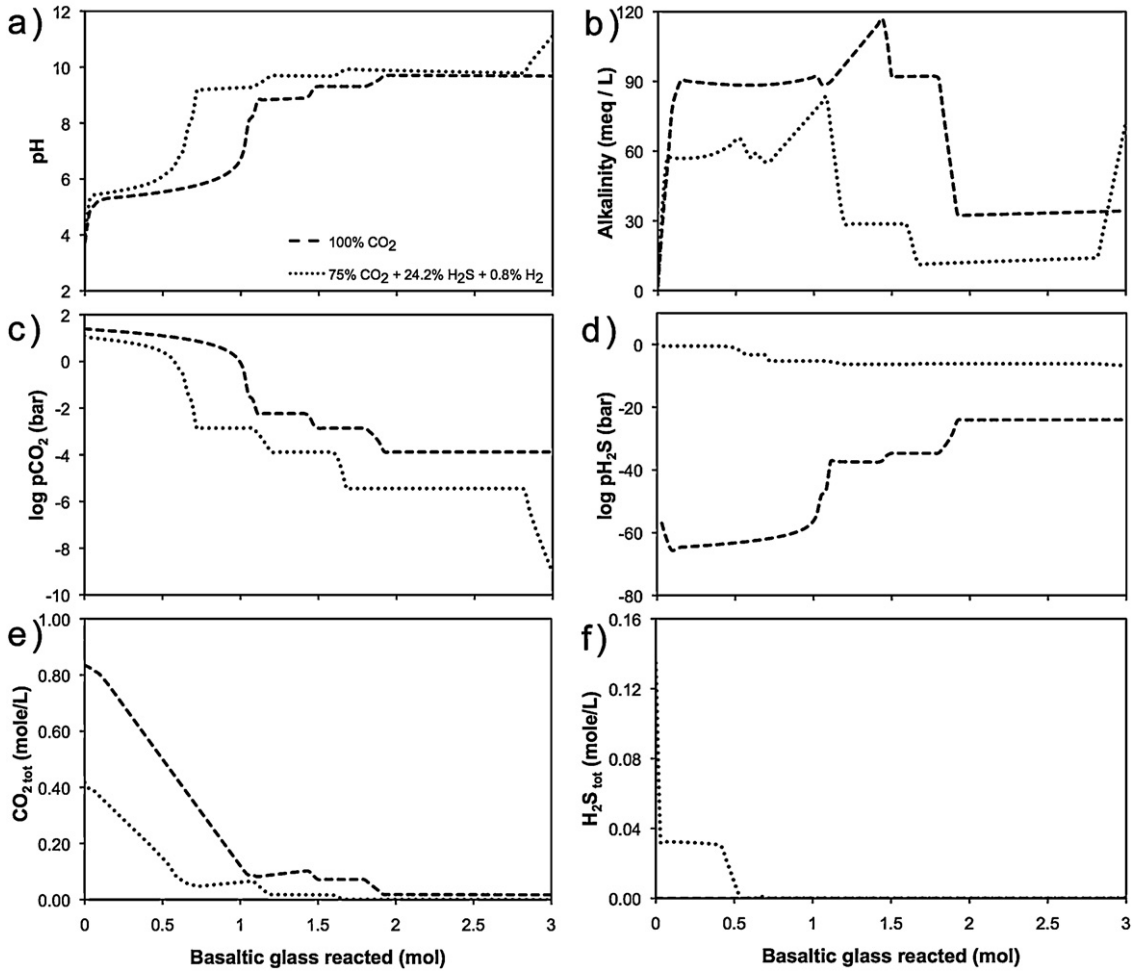

Fig. 13. Calculated chemical evolution of the fluid phase during reaction of water saturated with pure CO_2 and a CO_2–H_2S–H_2 gas mixture at 25 bars total pressure and 25 °C with basaltic glass (a) pH, (b) alkalinity, (c) partial pressure of CO_2, (d) partial pressure of H_2S, (e) total dissolved CO_2 and (f) total dissolved H_2S.

These models are in good agreement with previous studies of CO_2–basalt interactions, both in nature and in experiments. Reactive transport model of a pure CO_2 injection at the Carb-Fix site was done by Aradóttir et al. (2012). The model predicted all CO_2 sequestered in less than 10 years time. Calcite, and in lesser extent dolomite and Mg–Fe–carbonates formed close to the wells HN-4 and HK-34, few hundreds of meters away from the injection well. Rogers et al. (2006) showed that a time sequence of Fe/Mg-carbonates, dolomite with minor ankerite solid solutions and finally calcite, formed in the Nuussuaq, a basalt hosted petroleum reservoir in Greenland. Gysi and Stefánsson (2011) showed by numerical modeling and experimentation that CO_2–water–basalt interaction led to the sequential precipitation of Mg/Fe–carbonates, Ca–Mg–Fe–carbonates, then calcite. Associated minerals were Ca–Mg–Fe(III) smectite at low pH, followed by Ca–Mg–Fe(II) smectite, iron hydroxide, and zeolites. Other common secondary minerals found through the simulations were quartz/chalcedony, and Al–Si–minerals. Schaef et al. (2010) conducted supercritical CO_2–water–basalt interaction experiments at 60–100 °C and 62–103 bar. They observed the precipitation of various solid Ca–Mg–Fe–(Mn)–carbonate solid solutions, where Ca was the dominant cation. Adding H_2S to the experiments, resulted in co-precipitation of carbonate- and iron-sulphide coatings. In some cases pyrite precipitation inhibited the carbonation. This is in agreement with the model calculations described above and in Figs. 13 and 14. Stefánsson et al. (2011) modeled H_2S sequestration into basalt at geothermal conditions. The main secondary mineral formations calculated to precipiate were sulphide minerals and perhaps elemental sulfur formation at temperatures below 150 °C.

The volume of primary and secondary solids in these two model simulations is shown in Fig. 14e. and f. The calculations shown in these figures were performed assuming the rock porosity was 8%, consistent with the field observations summarized above. The dissolution of basaltic glass and precipitation of secondary minerals provokes a volume increase with time. The volume of the solids begins to exceed that of the initial rock after ~1 mole of basaltic glass has dissolved. This result suggests that pore clogging may be a factor, but only at some distance from the injection well.

One additional model calculation was performed in an attempt to validate these model calculations. This final calculation considers CO_2–water–basalt interaction at Hellisheidi *prior* to the gas injection. Such results can be directly compared with pre-injection water compositions. One kilogram of Hellisheidi shallow groundwater was equilibrated with atmospheric CO_2 at 30 °C and reacted with Stapafell basaltic glass as in the above calculations. The aqueous fluid initially had the composition of HK-13 water, a shallow well representing the upper groundwater system (Fig. 1). The composition of this water is given in Table 3 and contained 0.74 mmol/L of dissolved CO_2 at pH 8.07. Secondary minerals observed at the study site (see Table 1) were allowed to precipitate.

The calculated saturation state of the dissolved CO_2 and pH during this final and the previous two model calculations are shown in

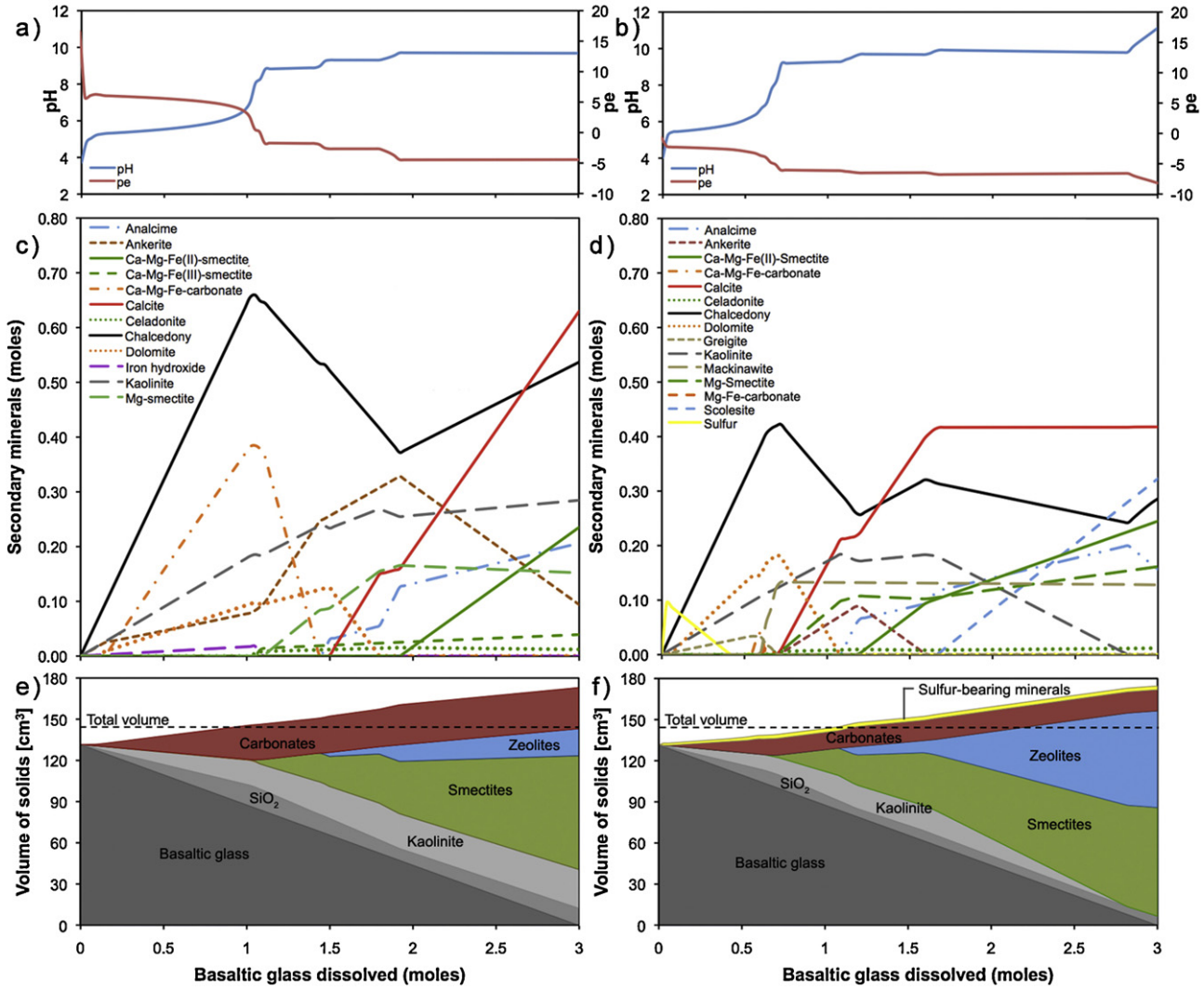

Fig. 14. Calculated chemical evolution of the fluid phase and solids during reaction of water saturated with pure CO_2 and a CO_2–H_2S–H_2 gas mixture at 25 bars total pressure and 25 °C with basaltic glass (a and b) fluid phase pH and pε; (c and d) mass of precipitated secondary minerals; (e and f) volume of solids. Plots on the left and right correspond to the evolution of the pure CO_2 and CO_2–H_2S–H_2 gas mixture equilibrated fluid, respectively. The total volume (e and f) calculation takes account the void fraction estimated for the field (Aradóttir et al., 2012), and is based on the complete dissolution of 3 moles of basaltic glass.

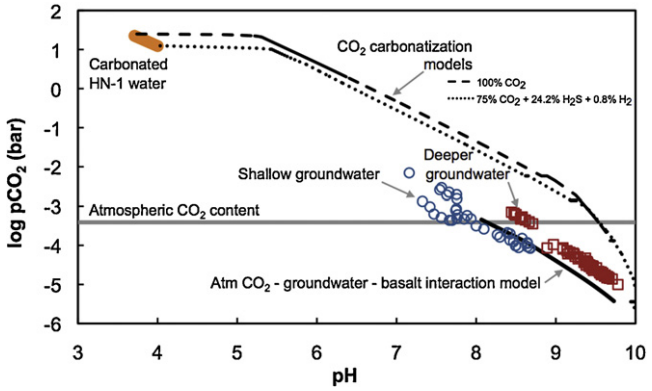

Fig. 15. Calculated and measured fluid phase CO_2 partial pressure (in a logarithmic scale) as a function of pH. Blue circles and red squares represent measured water compositions from the shallow and deep wells, respectively. The dotted curves show the calculated composition of the gas-charged waters during its interaction with basaltic glass. The gray horizontal line represents the atmospheric pCO_2. The solid black curve illustrates the evolution of atmosphere equilibrated HK-13 water reacted with basaltic glass. (For interpretation of the references to color in this figure legend, the reader is referred to the web version of this article.)

Fig. 15. Superimposed on the diagram are all the *in situ* compositions of all fluids collected in this study. When the HK-13 water is isolated from the atmosphere and prior to the precipitation of secondary minerals, basalt dissolution consumes protons, increases pH and lowers pCO_2 (Gislason and Eugster, 1987a, b; Oelkers and Gislason, 2001). With further water–basalt interaction, the CO_2 combines with divalent metals released from the basaltic glass to precipitate carbonate minerals (Gislason et al., 1993). The sampled groundwaters exhibit this same trend, though the measured pCO_2 is higher than that of the model in all the deep wells. The CO_2 partial pressure is especially high in well waters HK-7b, HK-13, and HK-26, which have a higher pCO_2 than the atmosphere. This may be due to the addition of deep CO_2 as also suggested by the stoichiometry of CO_2 *versus* Cl in Fig. 10. Note that the study area is only few kilometers away from the Hengill high-temperature geothermal field.

6. Conclusions

This study attests to the feasibility of using the studied Hellisheidi site specifically, and basaltic rocks in general, for the storage of carbon dioxide *via in situ* mineral carbonation. Carbon

storage in these rocks is supported by the existence of permeable layers containing waters that are isolated from the atmosphere and the abundance of divalent metal cations in the reactive host rocks. The ability of these rocks to form stable carbonate minerals is supported by the observation that calcite is currently forming at this site. Moreover, geochemical model calculations show that basalts are strongly undersaturated in CO_2 charged injection waters promoting their dissolution and that carbonate minerals readily become supersaturated as the basalt dissolves into these fluids. Geochemical model calculations suggest that adding H_2S gas to the injected gas mixture, results in rapid mineralization of both CO_2 and H_2S. Plans call for directly testing this possibility in the near future (Gislason et al., 2010; Aradóttir et al., 2011).

Acknowledgements

We would like to thank our friends and co-workers at the University of Iceland, in particularly Júlía K. Björke, Eydís S. Eiríksdóttir, Snorri Guðbrandsson, Iwona M. Galeczka, Kiflom G. Mesfin, Gabrielle Stockmann, Alexander Gysi, Nicole Hurtig, Mahnaz Rezvani Khalilabad, Domenik Wolff-Boenisch, Andri Stefánsson, Níels Óskarsson and Þorsteinn Jónsson for field- and lab assistance and fruitful discussions. We would also like to thank Einar Örn Þrastarson, Hólmfríður Sigurðardóttir, Edda Sif Aradóttir, Ingvi Gunnarsson and Bergur Sigfússon at Reykjavík Energy; Clare Desplats at CNRS, Toulouse; and Godfrey Fitton and Nic Odling at the Universty of Edinburgh. The Environmental Fund of Reykjavík Energy through the CarbFix project and the European Community through the MIN-GRO Research and Training Network (MRTN-CT-2006–035488) and the European R&D Project CARBFIX (FP7-ENERGY-2011-1-283148 CarbFix) are thanked for their financial support.

Appendix A. Supplementary data

Supplementary data associated with this article can be found, in the online version, at http://dx.doi.org/10.1016/j.ijggc.2012.11.019.

References

Alfredsson, H.A., 2007. Borehole HK-31 in Hellisheidi: petrology and alteration studies before CO_2 sequestration in basaltic rock. B.Sc. Thesis at the Department of Earth Sciences, University of Iceland (in Icelandic).

Alfredsson, H.A., Hardarson, B.S., Franzson, H., Gislason, S.R., 2008. CO_2 sequesration in basaltic rock at the Hellisheidi site in SW Iceland: stratigraphy and chemical composition of the rocks at the injection site. Mineralogical Magazine 72, 1–5.

Alfredsson, H.A., Wolff-Boenisch, D., Stefánsson, A., 2011. CO_2 sequestration in basaltic rocks in Iceland: Development of a piston-type downhole sampler for CO_2 rich fluids and tracers. Energy Procedia 4, 3510–3517.

Aradóttir, E.S.P., Sonnenthal, E., Bjornsson, G., Gunnlaugsson, E., Jonsson, H., 2009. Development of a coupled reactive fluid flow model for mineral CO_2 capture in Hellisheidi, Iceland. In: Paper Presented at the 2009 TOUGH Symposium Proceedings, Berkeley, CA, 14–16 September.

Aradóttir, E.S., Sigurdardóttir, H., Sigfússon, B., Gunnlaugsson, E., 2011. CarbFix: a CCS pilot project imitating and accelerating natural CO_2 sequestration. Greenhouse Gases: Science and Technology 1, 105–118, http://dx.doi.org/10.1002/ghg.18.

Aradóttir, E.S., Sonnenthal, E., Bjornsson, G., Jonsson, H., 2012. Multidimensional reactive transport modeling of CO_2 mineral sequestration in basalts at the Hellisheidi geothermal field, Iceland. International Journal of Greenhouse Gas Control 9, 24–40.

Árnason, B., 1976. Groundwater systems in Iceland traced by deuterium: Reykjavík. Societas Scientarium Islandica 42, 235.

Arnórsson, S., Andrésdóttir, A., 1995. Processes controlling the distribution of boron and chlorine in natural waters in Iceland. Geochimica et Cosmochimica Acta 59, 4125–4146.

Arnórsson, S., D'Amore F., Gerardo-Abaya J., 2000. Isotopic and geochemical techniques in geothermal exploration, development and use: sampling methods, data handling, interpretation. In: Arnórsson, S. (Ed.), International Atomic Energy Agency Publication, Vienna.

Arnórsson, S., Bjarnason, J.Ö., Giroud, N., Gunnarsson, I., Stefánsson, A., 2006. Sampling and analysis of geothermal fluids. Geofluids 6, 203–216.

Axelsson, G., Gunnarsson, G., 2009. Attempts at flow-rate estimates for keys wells of the Threngsli CarbFix project, wells HN-2 and 4. In: Iceland GeoSurvey, Reykjavík, report ÍSOR-09012.

Benning, L.G., Wilkin, R.T., Barnes, H.L., 2000. Reaction pathways in the Fe–S system below 100 °C. Chemical Geology 167, 25–51.

Björnsson, G., 2005. Vocabulary use, proceedings, methodology and definitions included in making conceptual- and computational models of the Hengill high-temperature fields (in Icelandic). In: Iceland GeoSurvey, Reykjavík, report ÍSOR-05203, 16 pp.

Broecker, W.S., Kunzig, R., 2008. Fixing climate. The story of climate science—and how to stop global warming. Green Profile.

Crovisier, J.L., Honnorez, J., Fritz, B., Petit, J.C., 1992. Dissolution of subglacial volcanic glasses from Iceland: laboratory study and modelling. Applied Geochemistry 1 (Suppl.), 55–81.

Einarsson, Þ., 1960. Geologie von Hellisheiði. Sonderveröffentlichungen Geol. Inst. D. Universität Köln Nr., 5.

Eiriksdottir, E.S., Louvat, P., Gíslason, S.R., Óskarsson, N., Harardóttir, J., 2008. Temporal variation of chemical and mechanical weathering in NE Iceland: evaluation of a steady-state model of erosion. Earth and Planetary Science Letters 272, 78–88.

Flaathen, T.K., Gislason, S.R., 2007. The effect of volcanic eruptions on the chemistry of surface waters: the 1991 and 2000 eruptions of Mt. Hekla volcano, Iceland. Journal of Volcanology and Geothermal Research 164, 293–316.

Flaathen, T.K., Oelkers, E.H., Gislason, S.R., 2008. The effect of aqueous sulphate on basaltic glass dissolution rates. Mineralogical Magazine 72, 39–41.

Flaathen, T.K., Gislason, S.R., Oelkers, E.H., 2009. Chemical evolution of the Mt. Hekla, Iceland, groundwaters: a natural analogue to CO_2 sequestration. Applied Geochemistry 24, 463–474.

Flaathen, T.K., Gislason, S.R., Oelkers, E.H., 2010. The effect of aqueous sulphate on basaltic glass dissolution rates. Chemical Geology 277, 345–354.

Flaathen, T.K., Oelkers, E.H., Gislason, S.R., Aagaard, P., 2011. The effect of dissolved sulphate on calcite precipitation kinetics and consequences for subsurface CO_2 storage. Energy Procedia 4, 5037–5043.

Franzson, H., Kristjánsson, B.R., Gunnarsson, G., Björnsson, G., Hjartarson, A., Steingrímsson, B., Gunnlaugsson, E., Gíslason, G., 2005. The Hengill–Hellisheiði geothermal field. Development of a conceptual geothermal model. In: Proceedings World Geothermal Congress, Antalya, Turkey, 24–29 April.

Franzson, H., Zierenberg, R., Schiffman, P., 2008. Chemical transport in geothermal systems in Iceland. Evidence from hydrothermal alteration. Journal of Volcanology and Geothermal Research 173, 217–229.

Franzson, H., Gudfinnsson, G.H., Helgadottir, H.M., 2010. Porosity, density and chemical composition relationships in altered Icelandic hyaloclastites. In: Birkle, P., Torres-Alvarado, I.S. (Eds.), Water-Rock Interaction XIII. CRC Press Inc., London, England, ISBN 978-0-415-60426-0.

Frolova, J., Ladygin, V., Franzson, H., Sigurdsson, O., Stefánsson, V., Shustrov, V., 2005. Petrophysical properties of fresh to mildly altered Hyaloclasitie Tuffs. In: Proceedings World Geothermal Congress, Antalya, Turkey, 24–29 April.

Gíslason, G., 2003. The effect of reinjected geothermal fluid on the groundwater—groundwater models for Hellisheidi (in Icelandic: Áhrif niðurrennslis jarðhitavatns á grunnvatn—Grunnvatnslíkan af Hellisheiði). In: Report GG-2003-04. Reykjavik Energy.

Gislason, S.R., Eugster, H.P., 1987a. Meteoric water-basalt interactions: I. A laboratory study. Geochimica et Cosmochima Acta 51, 2827–2840.

Gislason, S.R., Eugster, H.P., 1987b. Meteoric water-basalt interactions. II: a field study in N.E. Iceland. Geochimica et Cosmochimica Acta 51, 2841–2855.

Gislason, S.R., Arnórsson, S., 1990. Saturation state of natural waters in Iceland relative to primary and secondary minerals in basalts; fluid–mineral interactions: a tribute to H.P. Eugster. Spencer, R.J. I-Ming Chou (Eds.), Geochemical Society, Special Publication No. 2, pp. 373–393.

Gislason, S.R., Veblen, D.R., Livi, K.J.T., 1993. Experimental meteoric water-basalt interactions: characterization and interpretation of alteration products. Geochimica et Cosmochimica Acta 57, 1459–1471.

Gislason, S.R., Arnórsson, S., Ármannsson, H., 1996. Chemical weathering of basalt in SW Iceland: effects of runoff, age of rocks and vegetative/glacial cover. American Journal of Science 296, 837–907.

Gislason, S.R., Stefánsdóttir, M.B., Eiríksdóttir, E.S., 2000. ARCTIS, regional investigation of Arctic snow chemistry: results from the Icelandic expeditions, 1997–1999. In: Raunvísindastofnun, RH-05-2000, 48 pp.

Gislason, S.R., Snorrason, Á., Kristmannsdóttir, H.K., Sveinbjörnsdóttir, Á.E., Torsander, P., Ólafsson, J., Castet, S., Dupré, B., 2002. Effects of volcanic eruptions on the CO_2 content of the atmosphere and the oceans: the 1996 eruption and flood within the Vatnajokull Glacier, Iceland. Chemical Geology 190, 181–205.

Gislason, S.R., Oelkers, E.H., 2003. Mechanism, rates and consequences of basaltic glass dissolution: II. An experimental study of the dissolution rates of basaltic glass as a function of pH and temperature. Geochimica et Cosmochimica Acta 67, 3817–3832.

Gislason, S.R., Wolff-Boenisch, D., Stefansson, A., Oelkers, E.H., Gunnlaugsson, E., Sigurdardottir, H., Sigfusson, B., Broecker, W.S., Matter, J.S., Stute, M., Axelsson, G., Fridriksson, T., 2010. Mineral sequestration of carbon dioxide in basalt: a pre-injection overview of the CarbFix project. International Journal of Greenhouse Gas Control 4, 537–545.

Gislason, S.R., Hassenkam, T., Nedel, S., Bovet, N., Eiriksdottir, E.S., Alfredsson, H.A., Hem, C.P., Balogh, Z.I., Dideriksen, K., Oskarsson, N., Sigfusson, B., Larsen, G., Stipp, S.L.S., 2011. Characterization of Eyjafjallajökull volcanic ash particles and

a protocol for rapid risk assessment. Proceedings of the National Academy of Sciences of the United States of America 108, 7307–7312.
Goldberg, D.S., Takahashi, T., Slagle, A.L., 2008. Carbon dioxide sequestration in deep sea basalt. Proceedings of the National Academy of Sciences of the United States of America 105, 9920–9925.
Goldberg, D.S., Kent, D.V., Olsen, P.E., 2010. Potential on-shore and off-shore reservoirs for CO_2 sequestration in Central Atlantic magmatic province basalts. Proceedings of the National Academy of Sciences of the United States of America Sciences 107, 1327–1332.
Gudbrandsson, S., Wolff-Boenisch, D., Gislason, S.R., Oelkers, E.H., 2008. Dissolution rates of crystalline basalt at pH 4 and 10 and 25–75 °C. Mineralogical Magazine 72, 155–158.
Gudbrandsson, S., Wolff-Boenisch, D., Gislason, S.R., Oelkers, E.H., 2011. An experimental study of crystalline basalt dissolution from $2 \leq pH \leq 11$ and temperatures from 5 to 75° C. Geochimica et Cosmochimica Acta 75, 5496–5509.
Gysi, A.P., Stefánsson, A., 2008. Numerical modelling of CO_2–water–basalt interaction. Mineralogical Magazine 72, 55–59.
Gysi, A.P., Stefánsson, A., 2011. CO_2–water–basalt interaction. Numerical simulation of low temperature CO_2 sequestration into basalts. Geochimica et Cosmochimica Acta 75, 4728–4751.
Gysi, A., Stefánsson, A., 2012. CO_2–water–basalt interaction. Low temperature experiments and implications for CO_2 sequestration into basalts. Geochimica et Cosmochimica Acta 81, 129–152.
Hardarson, B.S., Helgadottir, H.M., Franzson, H., 2007. The Hellisheidi power plant. Injection site beside Grauhnukar. Iceland GeoSurvey, Reykjavík, report ÍSOR 2007/001 (in Icelandic).
Hardarson, B.S., Einarsson, G.M., Kristjánsson, B.R., Gunnarsson, G., Helgadóttir, H.M., Franzson, H., Árnason, K., Ágústsson, K., Gunnlaugsson, E., 2010. Geothermal Reinjection at the Hengill Triple Junction, SW Iceland. In: Proceedings World Geothermal Congress 2010, Bali, Indonesia, 25–29 April.
Helgadottir, H.M., Franzson, H., Sigurdsson, Ó., Ásmundsson, R.K., 2009. Hellisheidi—Hola HN-2. 1st, 2nd and 3rd stage: drilling for security casing down to 153 m, production casing down to 403 m and production part down to 2001 m depth. Iceland GeoSurvey, Reykjavík, report ÍSOR 2009/031 (in Icelandic).
Hunger, S., Benning, L.G., 2007. Greigite: a true intermediate on the polysulfide pathway to pyrite. Geochemical Transactions 8, 1.
IPCC, 2005. IPCC Special Report on Carbon Dioxide Capture and Storage, prepared by Working Group III of the Intergovernmental Panel on Climate Change. In: Metz, B., Davidson, O., de Coninck, H., Loos, C.M., Meyer, L.A. (Eds.), Cambridge University Press.
Jakobsson, S.P., Jónsson, J., Shido, F., 1977. Petrology of the Western Reykjanes Peninsula, Iceland. Journal of Petrology 19, 669–705.
Jakobsson, S.P., 1980. Outline of the petrology of Iceland. Jökull 29, 57–73.
Jakobsson, S.P., Moore, J.G., 1986. Hydrothermal minerals and alteration rates at Surtsey volcano, Iceland. Geological Society of America Bulletin 97, 648–659.
Jakobsson, S.P., Gudmundsson, M.T., 2008. Subglacial and intraglacial volcanic formations in Iceland. Jökull 58, 179–196.
Jones, J.G., 1966. Intraglacial volcanoes of southwest Iceland and their significance in the interpretation of the form of the marine basaltic volcanoes. Nature 212, 586–588.
Kelemen, P.B., Matter, J., 2008. In situ carbonation of peridotite for CO_2 storage. Proceedings of the National Academy of Sciences of the United States of America 105, 17295–17300.
Khalilabad, M.R., Axelsson, G., Gislason, S.R., 2008. Aquifer characterization with tracer test technique; permanent CO_2 sequestration into basalt, SW Iceland. Mineralogical Magazine 72, 121–125.
Kristmannsdóttir, H., Tómasson, J., 1978. Zeolite zones in geothermal areas in Iceland. In: Sand, L.B., Mumpton, F.A. (Eds.), Natural Zeolites: Occurrence, Properties, Use. Pergamon Press, Elmsford, New York, pp. 277–284.
Lackner, K.S., Wendt, C.H., Butt, D.P., Joyce, E.L., Sharp, D.H., 1995. Carbon dioxide disposal in carbonate minerals. Energy 20, 1153–1170.
Larsson, D., Grönvold, K., Oskarsson, N., Gunnlaugsson, E., 2002. Hydrothermal alteration of plagioclase and growth of secondary feldspar in the Hengill Volcanic Centre, SW Iceland. Journal of Volcanology and Geothermal Research 114, 275–290.
Le Quéré, C., Raupach, M.R., Canadell, J.G., Marland, G., Bopp, L., Ciais, P., Conway, T.J., Doney, S.C., Feely, R., Foster, P., Friedlingstein, P., Gurney, K., Houghton, R.A., House, J.I., Huntingford, C., Levy, P.E., Lomas, M.R., Majkut, J., Metzl, N., Ometto, J.P., Peters, G.P., Prentice, I.C., Randerson, J.T., Running, S.W., Sarmiento, J.L., Schuster, U., Sitch, S., Takahashi, T., Viovy, N., van der Werf, G.R., Woodward, F.I., 2009. Trends in the sources and sinks of carbon dioxide. Nature Geoscience 2, 831–836.
Matter, J.M., Kelemen, P.B., 2009. Permanent storage of carbon dioxide in geological reservoirs by mineral carbonation. Nature Geoscience 2, 837–841.
Matter, J.M., Broecker, W.S., Gislason, S.R., Gunnlaugsson, E., Oelkers, E.H., Stute, M., Sigurdardottir, H., Stefansson, A., Alfreðsson, H.A., Aradóttir, E.S., Axelsson, G., Sigfússon, B., Wolff-Boenisch, D., 2011. The CarbFix Pilot Project—storing carbon dioxide in basalt. Energy Procedia 4, 5579–5585.
McGrail, B.P., Schaef, H.T., Ho, A.M., Chien, Yi-Ju, Dooley, J.J., Davidson, C.L., 2006. Potential for carbon dioxide sequestration in flood basalts. Journal of Geophysical Research 111 (B12201), http://dx.doi.org/10.1029/2005JB004169.
Moore, J.G., Fabbi, B.P., 1971. An estimate of the juvenile sulfur content of basalt. Contributions to Mineralogy and Petrology 33, 118–127.
Moore, J.G., Calk, L.C., 1991. Degassing and differentiation in intraglacial volcanoes, Iceland. Journal of Volcanology and Geothermal Research 46, 157–180.
Mutonga, M.W., Sveinbjornsdottir, A., Gislason, G., Armansson, H., 2010. The isotopic and chemical characteristics of geothermal fluids in Hengill Area, SW-Iceland (Hellisheidi, Hveragerdi and Nesjavellir Fields). In: Proceedings World Geothermal Congress 2010, Bali, Indonesia, 25–29 April, p. 2010.
Oelkers, E.H., Gislason, S.R., 2001. The mechanism, rates, and consequences of basaltic glass dissolution: I. An experimental study of the dissolution rates of basaltic glass as a function of aqueous Al, Si, and oxalic acid concentration at 25 °C and pH = 3 and 11. Geochimica et Cosmochimica Acta 65, 3671–3681.
Oelkers, E.H., Cole, D.R., 2008. Carbon dioxide sequestration: a solution to a global problem. Elements 4, 305–310.
Oelkers, E.H., Gislason, S.R., Matter, J., 2008. Mineral carbonation of carbon dioxide. Elements 4, 333–337.
Oelkers, E.H., Gislason, S.R., 2010. Water–CO_2–rock interaction during carbon sequestration. European Mineralogical Union Notes in Mineralogy 10, 325–344.
Oskarsson, N., Sigvaldason, G.E., Steinthórsson, S., 1982. A dynamic model of rift zone petrogenesis and the regional petrology of Iceland. Journal of Petrology 23, 28–74.
Parkhurst, D.L., Appelo, C.A.J., 1999. User's guide to PHREEQC (Version 2)—a computer program for speciation, batch-reaction, one-dimensional transport, and inverse geochemical calculations: U.S. In: Geological Survey Water-Resources Investigations Report 99-4259, 312 p.
Rogers, K., Neuhoff, P., Pedersen, A., Bird, D., 2006. CO2 metasomatism in a basalt hosted petroleum reservoir, Nuussuaq, West-Greenland. Lithos 92, 55–85.
Rutqvist, J., Birkholzer, J., Cappa, F., Tsang, C.-F., 2007. Estimating maximum sustainable injection pressure during geological sequestration of CO_2 using coupled fluid flow and geomechanical fault-slip analysis. Energy Conversion and Management 48, 1798–1807.
Saemundsson, K., 1967. Vulkanismus und Tektonik des Hengill-Gebietes in Suidwest-Island. Acta Naturalia Islandica 2, 105.
Saemundsson, K., 1995. Hengill, Geological Map (Bedrock) 1:50. 000. National Energy Authority and Iceland Geodetic Survey.
Saemundsson, K., 2003. Hellisheidi power plant: geological conditions within the utilization area. In: Report KS 03/02, Iceland GeoSurvey, Reykjavík, 2003 (in Icelandic).
Schaef, H.T., McGrail, B.P., 2009. Dissolution of Columbia River Basalt under mildly acidic conditions as a function of temperature: experimental results relevant to the geological sequestration of carbon dioxide. Applied Geochemistry 24, 980–987.
Schaef, H.T., McGrail, B.P., Owen, A.T., 2010. Carbonate mineralization of volcanic province basalts. International Journal of Greenhouse Gas Control 4, 249–261.
Sigurdsson, F., Einarsson, K., 1988. Groundwater resources of Iceland—availability and demand. Jökull 38, 35–53.
Sigurdsson, Ó., Stefánsson, V., 1994. Reservoir parameters—measurements from rock core (in Icelandic). National Energy Authority, OS-94049/JHD-28 B.
Sigvaldason, G.E., Óskarsson, N., 1976. Chlorine in basalts from Iceland. Geochimica et Cosmochimica Acta 40, 777–789.
Sigvaldason, G.E., Óskarsson, N., 1986. Fluorine in basalts from Iceland. Contribution to Mineralogy and Petrology 94, 263–271.
Stefánsson, A., Gunnarsson, I., Giroud, N., 2007. New methods for the direct determination of dissolved inorganic, organic and total carbon in natural waters by reagent-FreeTM Ion chromatography and inductively coupled plasma atomic emission spectrometry. Analytica Chimica Acta 582, 69–74.
Stefánsson, A., Arnórsson, S., Gunnarsson, I., Kaasalainen, H., Gunnlaugsson, E., 2011. The geochemistry and sequestration of H_2S into the geothermal system at Hellisheidi, Iceland. Journal of Volcanology and Geothermal Research 202, 179–188.
Stockmann, G.J., Wolff-Boenisch, D., Gislason, S.R., Oelkers, E.H., 2008. Dissolution of diopside and basaltic glass: the effect of carbonate coating. Mineralogical Magazine 72, 135–139.
Stockmann, G.J., Wolff-Boenisch, D., Gislason, S.R., Oelkers, E.H., 2011. Do carbonate precipitates affect dissolution kinetics? 1: Basaltic glass. Chemical Geology 284, 306–316.
Stroncik, N.A., Schmincke, H.-U., 2001. Evolution of palagonite: crystallization, chemical changes, and element budget. Geochemistry, Geophysics, Geosystems 7, 1017.
Stumm, W., Morgan, J.J., 1996. Aquatic Chemistry: Chemical equilibria and rates in natural waters, third ed. John Wiley & Sons, New York, 1022 p.
Sveinbjörnsdóttir, Á.E., Johnsen, S.J., 1992. Stable isotope study of the groundwater system in the Thingvallavatn area. Oikos 64, 136–150.
Sveinbjörnsdóttir, A., Heinemeier, J., Arnórsson, S., 1995. Origin of ^{14}C in Icelandic groundwater. Radiocarbon 37, 551–565.
Thorarinsson, S.B., Helgadottir, H.M, Franzson, H., Hardarson, B.S., Hjartarson, A., Ásmundsson, R.K., Sigurdsson, G. 2006. Hellisheidi—Borehole HN-4. 1–3rd stage: Drilling for 18 5/8"ecurity casing down to 105 m, 13 3/8"roduction casing down to 400 m, and 12 1/4"roduction part down to 1204 m depth. Iceland GeoSurvey, Reykjavík, report ÍSOR 2006/055 (in Icelandic).
Wolff-Boenisch, D., Gislason, S.R., Oelkers, E.H., 2006. The effect of crystallinity on dissolution rates and CO_2 consumption capacity of silicates. Geochimica et Cosmochimica Acta 70, 858–870.
Wolff-Boenish, D., Wenau, S., Gislason, S.R., Oelkers, E.H., 2011. Dissolution of basalts and peridotite in seawater, in the presence of ligands, and CO_2: implications for mineral sequestration of carbon dioxide. Geochimica et Cosmochimica Acta Acta 75, 5510–5525.